EMBRY-RIDDLE
Aeronautical University™
SCHOLARLY COMMONS

Dissertations and Theses

12-2017

Mechanical and Electrical Characterization of Carbon Fiber/Bucky Paper/Zinc Oxide Hybrid Composites

Suma Ayyagari

Follow this and additional works at: https://commons.erau.edu/edt

Part of the Aerospace Engineering Commons

MECHANICAL AND ELECTRICAL CHARACTERIZATION OF CARBON FIBER /

BUCKY PAPER /ZINC OXIDE HYBRID COMPOSITES

A Thesis

Submitted to the Faculty

of

Embry-Riddle Aeronautical University

by

Suma Ayyagari

In Partial Fulfillment of the

Requirements for the Degree

of

Master of Science in Aerospace Engineering

December 2017

Embry-Riddle Aeronautical University

Daytona Beach, Florida

MECHANICAL AND ELECTRICAL CHARACTERIZATION OF CARBON FIBER / BUCKY PAPER /ZINC OXIDE HYBRID COMPOSITES

by

Suma Ayyagari

A Thesis prepared under the direction of the candidate's committee chairman, Dr. Marwan Al-Haik, Department of Aerospace Engineering, and has been approved by the members of the thesis committee. It was submitted to the School of Graduate Studies and Research and was accepted in partial fulfillment of the requirements for the degree of Master of Science in Aerospace Engineering.
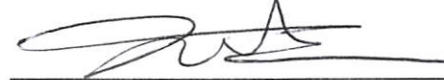
THESIS COMMITTEE
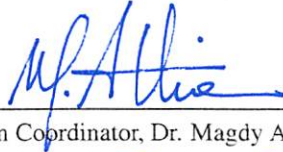
_____
Chairman, Dr. Marwan Al-Haik

_____
Member, Dr. Daewon Kim

_____
Member, Dr. Sirish Namilae

_____   12.5.2017
Graduate Program Coordinator, Dr. Magdy Attia   Date

_____   12/5/2017
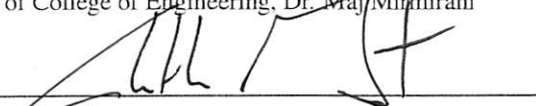Dean of College of Engineering, Dr. Maj Mirmirani   Date

_____   12/5/2017
Vice Chancellor, Academic Support, Dr. Christopher Grant   Date

ACKNOWLEDGMENTS

It gives me pleasure to acknowledge the people for all the support and strength they gave me which made this thesis possible.

I would like to thank Dr. Marwan Al-Haik for his guidance and moral support. The stress-free working relationship he fostered was the key for the success of this work.

I thank my committee members, Dr. Daewon Kim and Dr. Sirish Namilae for always lending me a helping hand when needed. I appreciate them taking time for reviewing my work.

Also, I would like thank my friends and family for their immense belief in me. I would specially like to thank Dr.Rollins for her help with the microscope.

Lastly, I thank the university for the financial support and the lab space. This work would have been impossible without proper equipment.

TABLE OF CONTENTS

LIST OF TABLES

LIST OF FIGURES

Figure | Page

ABBREVIATIONS

CNT	Carbon nanotubes
ZnO	Zinc oxide
CF	Carbon Fiber
BP	Bucky paper
CFRPs	Carbon fiber reinforced plastics
DMA	Dynamic material analysis
MWCNTs	Multi walled carbon nanotubes
SWCNTs	Single walled carbon nanotubes
SF	Surface Resistivity
C-C	Carbon-carbon
ILSS	Inter-laminar shear strength
SEM	Scanning electon microscope
MGS	Mean grain size
ZCD	Zinc acetate dihydrate

ABSTRACT

Ayyagari, Suma MSAE, Embry-Riddle Aeronautical University, December 2017. Mechanical and Electrical Characterization of Carbon Fiber / Bucky paper /Zinc Oxide Hybrid Composites.

The quest for multifunctional carbon fiber reinforced composites (CFRPs) expedited the use of several nano reinforcements such as zinc oxide nanorods (ZnO) and carbon nanotubes (CNTs). Zinc oxide is semi-conductor with good piezoelectric and pyroelectric properties. These properties could be transmitted to CFRPs when a nanophase of ZnO is embedded within CFRPs. In lieu of ZnO nanorods, Bucky paper comprising mat of multiwall-carbon nanotubes (MWCNTs) could be sandwiched in-between laminae to construct a functionally graded composite with elevated electrical and thermal conductivities. In this study, a low temperature ($90°$C) hydrothermal synthesis method was utilized to grow ZnO nanorods on the surface of carbon fiber fabrics. Different configurations of hybrid composites based on carbon fibers, in combination with ZnO nanorods and Bucky paper were fabricated. The composites were tested mechanically via tensile and dynamic mechanical analysis (DMA) tests to examine the effect of the different nanoadditives on the stiffness, strength and damping performance of the hybrid composites. Surface electrical resistivities of the hybrid composites were probed to examine the contributions of the different nanoadditives. The results suggest that there are certain hybrid composite combinations that could lead to the development of highly multifunctional composites with better strength, stiffness, damping and electrical conductivity.

1. Introduction

Composites comprise two or more materials combined on a macroscopic scale to form a third useful material (Jones, 1998). The main constituents of a composite are fiber and matrix as shown in Figure 1.1. The strength of the constituents individually and their bonding determine the total strength and load carrying capacity of the composite.
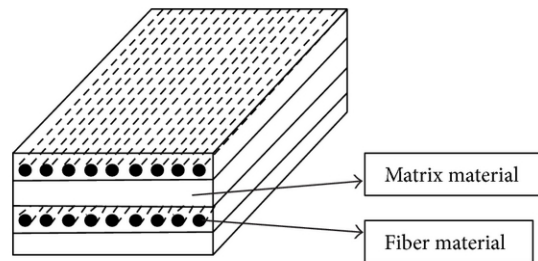
Figure 1.1: Composite constituents (Jones, 1998)

1.1 Carbon Fiber Reinforced Plastics (CFRP)

Carbon fiber-reinforced plastics (CFRPs) are made of polymer matrix reinforced with fibers. The various fibers used in industry include glass, carbon, aramid, paper, wood, asbestos and others. The polymers in use are epoxy, vinylester, polyester thermosetting plastic, or phenol formaldehyde resins, among others. (Alberto, 2013) Carbon fiber, in particular is used in applications where fatigue resistance, elevated strength and electri-

cal conductivity are required. Also, CFRPs have less than 2-3% strain to failure and are available in standard, intermediate and high stiffness.
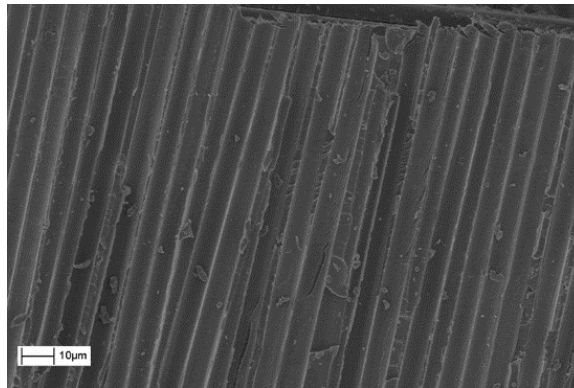
(a) Top View
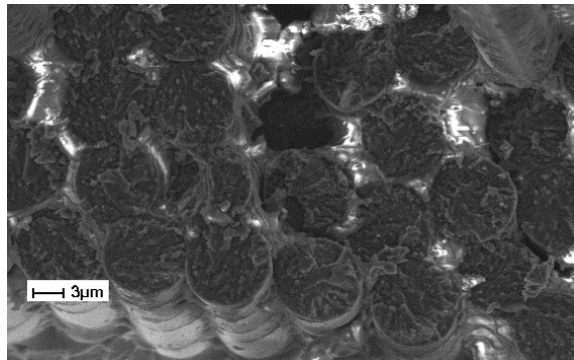
(b) Cross-Sectional View

Figure 1.2: Fiber Views in CFRP [Unpublished Work, Dr.Al Haik]

CFRPs possess various advantages which include the high strength to weight ratio, stiffness to weight ratio, high utilization factor, chemical and fatigue resistance, ease of formability, and higher performance. The applications of CFRPs are seen in various domains like automobiles, marine, aeronautical, communication, military and many more. Finally, they have a few disadvantages which include the high cost of raw material, skilled manufacturing techniques, sparse repair and recycling techniques, and out of plane mechanical properties in the finished products. The molds required for making products with

CFRPs in bulk manufacturing need skilled labor which significantly increases the initial cost. In a repair scenario, the conventional materials like steel and aluminum are easy to work with. Research is still in progress to study the behavior of fibers in CFRPs during crack propagation and thus, patching techniques are yet to be established. Composite parts are replaced currently in case of an incident. This results in high maintenance cost. Similar is the case with recycling.

1.2 Hybrid Composites

Hybrid composites have evolved due to the need to enhance the interlaminar strength in the CFRPs. These composites are made by the addition of nanoreinforcements to the matirx or by growing nano phase on the fibres. Apart from better mechanical and in-plane properties, these composites possess multi-functional properties based on the procedures being performed to incorporate the nano phase. Various synthesis methods will be discussed in the literature review.
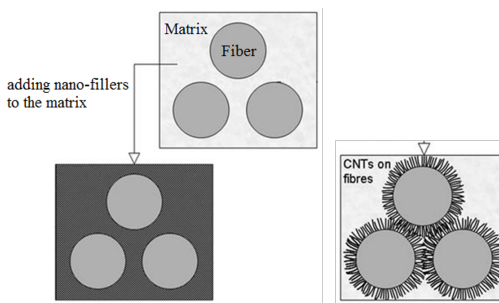
Figure 1.3: Hybrid composites Preparation Methods

1.3   Importance of ZnO Nanotubes and Buckypaper

Zinc oxide (ZnO) is a material of high importance due to its combined piezoelectric, pyroelectric and semiconducting properties since 1960s. These properties result from the unique asymmetrical structure of wurtzite Figure (1.4), large electromechanical coupling, and high exciting band energy respectively. Thus, this material has a wide range of applications including optoelectronics, sensors, transducers and catalysis.
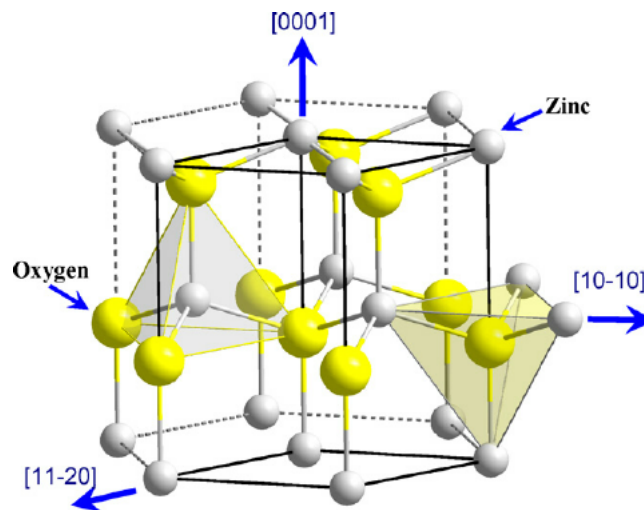
Figure 1.4: ZnO wurtzite structure and planes (Fu et al., 2010)

ZnO is also known for various possible growth morphologies depending on the surface structure orientation chosen for the procedure. The rapid directions for growth in ZnO include $\langle 2\bar{1}\bar{1}0\rangle, \langle 01\bar{1}0\rangle\, and \pm [0001]$. Growth is also controlled by various parameters like temperature, pressure, surface diffusion, time and various other factors(Ma, Wang, Kong, Jia, & Wang, 2015). The different kinds of possible ZnO structures include nanocombs, nanobelts, branched hierarchial structures, nanohelixes, nanorods, and nanorings as shown in Figure 1.5.
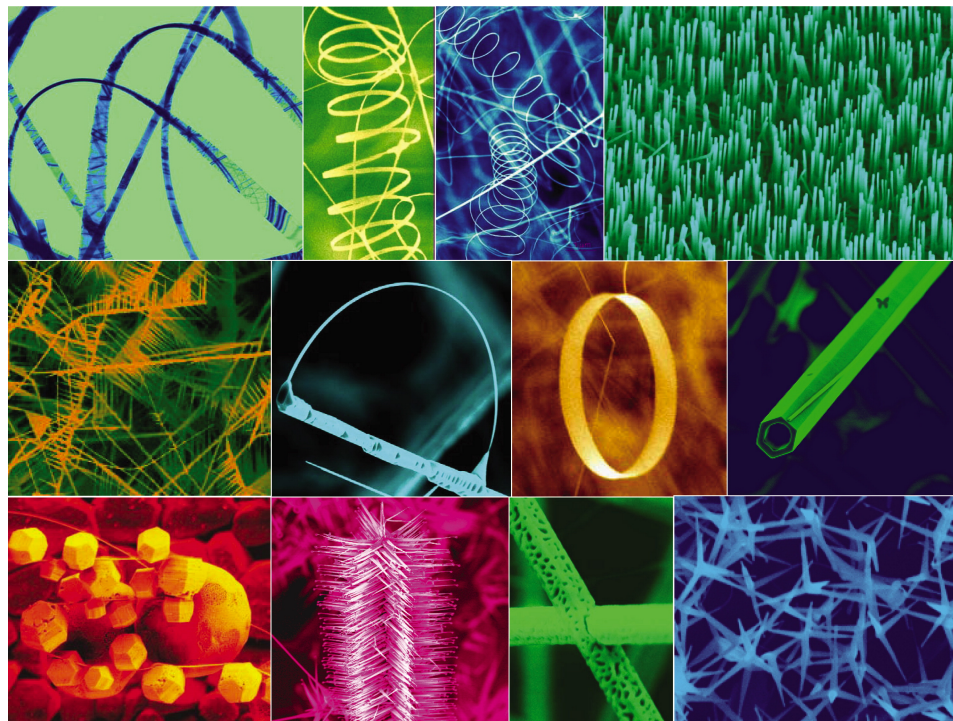
Figure 1.5: Various nanostructures of ZnO (Wang, 2004)

There are various methods to synthesize these nanostructures. These include vapor deposition methods, wet-chemical synthesis methods such as sol-gel, electrodeposition, and low temperature aqueous chemical growth methods (Byrne et al.,2011), (Hung & Whang, 2003), (Liu et al., 2016), and (Akgun et al., 2012). The vapor deposition method which is frequently used for highly controlled and perfect nanostructures, involves deposition of Zinc and Oxygen vapors on the required substrate where they react to form ZnO. However, this procedure requires expensive equipment, elevated temperatures, special substrates and source materials. Thus, the cost, and the preference of lower temperature synthesis for carbon fiber substrate led to the selection of aqueous chemical growth method in the current research.

Buckypaper, known as a novel material for aerospace industry promises multifunctional advanced structures. It is 10 times lighter than steel when being 250 times stiffer at the same time. It is a mat of carbon nanotubes (CNTs) which are extremely thin even in comparison to human hair. Further, it is as conductive as copper and comparable to steel in heat dissipation. Incorporation of Buckypaper, as a ply layer in composites made of carbon fiber has the capacity to increase the overall mechanical and conductive properties of the resulting structure. Thus, in this thesis, the combined effect of Buckypaper and ZnO nanorods in a hybrid composite will be analyzed.

1.4 Thesis Proposal

This research is an attempt to fabricate and characterize a hybrid composite with enhanced mechanical, and electrical properties. Various references were suggested using CNTs as a matrix filler, or growing nanorods of various oxides on Carbon Fiber, employing various procedures for growth in each case. These are discussed in detail in the next section. But the combined effect of Buckypaper and ZnO nanorods together is yet to be explored in detail since this involves enhancement of both matrix and fiber at the same time. Thus, in the current work, various configurations of two-layer composites were made with combinations of ZnO nanorods and Buckypaper with carbon fiber. This is followed by characterization through various analysis which includes tensile testing, dynamic material analysis (DMA), fracture analysis and electrical conductivity test. The results were analyzed and conclusions were drawn on how their stiffness, strength, and conductivity parameters vary as a result of different nano fillers.

2. Literature Review

Enhancement of stiffness and strength in composites has been an active research area since the realization of their wide application scope. One of the many investigators include Kowbel et al. (Kowbel et al., 1996) whose work aimed at increasing the laminar shear strength in carbon-carbon composites. This was attempted through whiskerization of pre heated carbon fabric using SiO which formed SiC whiskers with varied areal density. Scanning and transmission electon microscopy techniques were used to study surface morphologies of the modified carbon fabric and the micro-structure of the SiC whiskers, respectively. This study observed a reduction in flexural strength of C-C composites with increase in SiC whiskers. Also, fiber surface pittng and defected β-SiC were observed in the microstructure analysis. Thus, it was concluded that significant increase in interlaminar shear strength (around 300%) was possible with low whiskerized fabric without compromising the flexural strength.

Recently, carbon nanotubes (CNTs) were widely used to improve the carbon fiber composite properties. Liu et al. (W. Liu et al., 2015), fabricated carbon nano-tube carbon fiber, also called a hybrid fiber by sizing unsized unidirectional carbon fiber with a polyphthalazinone ether ketone (PPEK) sizing agent containing CNTs. Three point bending test was performed to determine the inter-laminar shear strength (ILSS), drop tests to measure impact toughness and SEM analysis to study fracture surface. Along with improvement

in wetting performance with the resin used, an increase in ILSS by 115.4% and impact toughness by 27% was observed in the resulting composites. However, improvements in other mechanical properties were limited.

Carbon nanotubes (CNTs) (Iijima, 1991) are unique allotrope of carbon visualized by considering a single graphene sheet (representing a lattice of carbon atoms distributed in a hexagonal pattern) rolled into a tube (Sinnott & Andrews, 2001). The appealing properties of CNTs, typically 1 to a few nm in diameter, are attributed to their unique and minimal defect nanostructure. Single wall carbon nanotubes (SWCNTs) possess exceptional mechanical, thermal, and electric properties compared to macroscale fibers such as graphite, Kevlar, SiC and alumina (Dresselhaus et al., 2004). The extraordinary mechanical, electrical, and thermal properties of CNTs have spurred investigations to utilize these nano-scale structures as a reinforcement phase in composites to enhance the properties of the host matrix. A wealth of studies have been published since the discovery of the multiwall carbon nanotubes (MWCNTs) in 1991 on utilizing them for different applications including, but not limited to, structural, thermal, electromagnetic, electroacoustic, chemical, and electrical circuits (Baughman et al., 2002). The strength, stiffness and the fracture properties of CNTs are orders of magnitudes higher than most common structural materials used in civilian and military applications (Erik & Tsu-Wei, 2002). For example, an epoxy nanocomposite based on MWCNTs ($\approx 2\%$ volume fraction) showed an increase in Young's modulus and yield strength by 100% and 200%, respectively and nine orders of magnitude improvement in the electrical conductivity compared to the neat epoxy (Allaoui

et al., 2002). Moreover, CNTs reinforcement increases the toughness of the composite to absorb impact energy due to their highly elastic behavior during loading.

Researchers have attempted to incorporate CNTs in polymer matrices with limited success due to the extreme difficulty in uniformly dispersing CNTs in polymeric matrices because of the large surface area of CNT (Erik & Tsu-Wei, 2002). The high-aspect ratio CNTs tend to entangle and form agglomerates when dispersed into a matrix (e.g., polymer). Rather complicated chemical and physical routes should be employed to moderately disentangle CNTs and disperse them into the matrix. These chemo-physical processes could damage the CNT covalent bonds, or induce undesired functionalizing to it and / or removing CNTs semispherical end caps. Sonication (Allaoui, Bai, Cheng, & Bai, 2002) and calendaring (Y. L. Li et al., 2004) have been utilized considerably to alleviate this problem, but are not effective beyond ≈ 3.0 wt % CNT volume fraction due to the formation of aggregates (Y. L. Li, Kinloch, & Windle, 2004). A combination of dispersion and extrusion techniques have been reported in the literature for producing CNTs composites (Y. L. Li et al., 2004) with tailored microstructure, e.g. aligned CNTs. However, in both dispersion and extrusion techniques, producing uniform and well-dispersed CNTs composite is difficult because of the small amount of solid powder (carbon) compared with the large amount of liquid polymer (matrix) in early mixing stages. This often leads to phase separation due to the strong Van der Waals attractions amongst the CNTs bundle compared with that between the CNTs and the polymer matrix (Garmestani et al., 2003). Furthermore, excessive sonication of SWCNTs toward better dispersion might result in breaking them into

shorter tubes and thus reducing their aspect ratio (Zeineldin et al., 2009) and, consequently, negatively affects their corresponding composites performance.

2.1 Evolution of hybrid composites

To exploit the remarkable properties of both CFRPs and CNTs, hybrid carbon fiber reinforced CNT-polymer were developed (Alipour Skandani et al., 2012). However, the inadequacies with the dispersion of CNTs into the matrix were present. Alternatively, to eliminate the need for dispersion and deagglomeration, CNTs can be controlled-grown on the surfaces where they are needed. CNTs can be grown on most substrates such as silicon, silica, and alumina (Garcia et al., 2008). However, there are fewer reports discussing the CNTs growth on carbon materials; in particular yarns and fabrics (Otsuka et al., 2004). Two challenges in CNTs growth on carbon substrates are (i) transition metals (i.e. catalysts for CNTs synthesis) are easily diffused into the carbon substrates and, (ii) the different phases of carbon materials are able to form on the graphite substrates because the growth conditions are similar to the diamond or diamond-like carbon growth (Zhu et al., 2003).

Catalytic chemical vapor deposition (CCVD) has been broadly utilized to grow carbon nanofilaments on the surface of carbon fiber yarns with the aid of catalysts such as nickel, iron, cobalt and palladium at temperatures ranging from 700 to 1100°C (Sinnott & Andrews, 2001), (Gibson, 2010), (Luhrs et al., 2009), (Al-Haik et al., 2010), (Boskovic et al., 2005), (Garcia et al., 2008), (Phillips et al., 2007) and (Chen et al., 2011). However, the temperature needed for the growth of CNTs utilizing CCVD is rather high and is destructive to the substrate carbon fiber strength itself (Zhang et al., 2009); (Westwood et al.,

1996). For example, Thostenson et al. (Erik & Tsu-Wei, 2002) utilized CVD (at 700 °C) to grow CNTs on carbon fibers then fabricated a composite based on them. They reported that the exposure to growth conditions resulted in significant degradation of the fiber/matrix interface. Similarly, Zhang et al. (Zhang et al., 2009), upon utilizing CVD (at 700-800 °C) to grow CNTs on PAN carbon fibers, reported that the strength of the T650 fiber was reduced by nearly 40% due to the exposure to elevated temperatures. While the fiber dominated properties of the CFRPs were shown to degrade due to the exposure to the high CCVD temperatures, the interlaminar properties (e.g. interlaminar shear strength) of the composites containing CCVD grown CNTs was reported to improve (Askari Ghasemi-Nejhad, 2011) and (Wicks et al., 2010).

Recently, Tehrani et al (Tehrani et al., 2013) utilized graphitic structure by design (GSD) synthesis at relatively lower temperature ($\approx 500°C$) to grow MWCNTs over the surface of PAN-based carbon fibers. Compared to the carbon fiber/epoxy composite, results showed a slight decrease in the composite tensile strength (3.4%) and an improvement of the Youngs modulus (8.17%). However, more pronounced enhancements were reported for the DMA loss modulus (120%). Also, computational models were developed using Monte Carlo percolation method to study how the variation of CNT and graphene nanoplatelet (GNP) fillers change electrical and piezoresistive properties of hybrid composites (Gbaguidi, Namilae, & Kim, 2017) .

Hybrid composites are usually made by adding nano-fillers to either matrix or growing nano structures on fibers. The current research is more focused on the latter. Deka et al., (Deka et al., 2016), utilized a technique which involves both. Copper oxide (CuO)

nano-paritcles on woven carbon fiber were synthesized from copper nitrate and hexam-ethylenetetramine via microwave green synthesis, in addition to Graphene Oxide which was produced by modifying Hummer's method and dispersed in the resin. These components are further used to make polyester composites via a vacuum-assisted resin transfer molding (VARTM) process. This procedure significantly improved the tensile strengths and modulus by 61.2% and 57.5%, respectively. Enhancement in composite elasticity and impact energy absorption capacity were noticed. Finally, inter-laminar resistive heating of the composite laminate was increased with a slower cooling rate.

Like CNTs, zinc oxide (ZnO) nanowires (NWs) can be grown on carbon fibers surface to enhance the interface between the fibers and the matrix. Zinc oxide species (tubes, belts, particles, films, wires, etc.) possess semiconductor and piezoelectric properties which makes them well-suited for a variety of applications from solar cells, sensors, structural applications, to energy harvesting devices (Awan et al., 2012); (Gullapalli et al., 2010). Different synthesis protocols were developed to grow ZnO nanostructures such as vapor-phase transport, metallorganic chemical vapor deposition (MOCVD), sputtering, molecular beam epitaxy (MBE), thermal evaporation and vapor-liquid-solid (VLS) (Wagner & Ellis, 1964). These techniques are time-consuming and / or require elevated synthesis temperatures which limit their potential use for industrial applications.

Unlike CNTs, despite their extraordinary physical properties, there are fewer reports on the effect of ZnO as interfacial reinforcement for FRPs. Allington et al. (Allington et al., 1998) tested the shear strength of a single carbon fiber wrapped with ZnO NWs and reported 113% increase in the interfacial shear strength. Ehlert et al. (Ehlert & Sodano, 2009)

utilized identical ZnO growth process on aramid fiber and suggested that the carboxylic acid group is responsible for the good interfacial shear strength between the ZnO NWs and the carbon fiber. More recently, (Skandani et al., 2012) reported 50% enhancement in the CFRPs loss modulus upon growing ZnO NWs on the interface. This improvement was attributed to the increased interfacial area between the NWs and the epoxy matrix. However, such enhancement was accompanied with a slight decrease in the storage modulus ($\approx$ 7.0%).

Although there are various studies on the topics mentioned above, the current research is more focused on ZnO nano-rod growth on carbon fiber. Thus, the research involving various processing methods and their analysis is thoroughly studied in the following works. (Byrne, McGlynn, Cullen, & Henry, 2011) investigated a technique for growth of aligned ZnO nanorods at high temperature aiming to eliminate the limitations of epitaxially matched substrates and use of catalysts. Nonosphere lithography, in combination with chemical bath deposition and vapour phase transport were used to be finally called catalyst-free inverse nanosphere lithography method. As a result, aligned c-axis ZnO nanorods with controlled density and spacing were observed in addition to excellent optical properties for usage in optoelectronic applications. However, the high temperature exposure of the substrate is a limitation in this procedure.

Hung and Whang (Hung & Whang, 2003) proposed a low temperature growth technique for single crystal ZnO nanorods growth on nanostructured substrates in two steps. First, sol-gel reaction is used to form uniform ZnO nanoparticle colloids with the reaction of cetyltrimethylammonium hydroxide (CTAOH) added to the stirred solution of zinc

acetate and ethanol. Secondly, these colloids were dipped into heat treated glass substrates (Figure 2.1). These substrates were then immersed in equimolar of zinc nitrate and methenamine aqueous solutions for 24 hours at 90°C to promote large scale nanorods growth of around 45nm (in diameter). This is a low cost technique which has potential applications in optoelectronic nanodevices. (Liu et al., 2016) suggested a similar method with a slight variation in the method of producing nanofibers. Electrospinning method was used for the preparation of polymer nanofibers from various zinc salts which are then deposited on glass substrate. Calcination followed by hydrothermal growth in a nutrient solution resulted in a dense and more organized nanowires (Figure 2.2). The various parameters like length, diameter, and morphologies could be controlled by changing the reaction parameters like incubation time and concentration of zinc salts.

Tak and Yong (Tak & Yong, 2005) proposed a multi-step procedure for the growth of patterned and more controlled nanorods on a silicon substrate. Thermal evaporation was used to deposit thin ZnO metal seed layer on the substrate This was followed by the growth of nanorods in an aqueous solution of zinc nitrate and ammonia. Then, the patterning of the substrate was carried out using photolithography technique (Figure 2.3). This method seemed promising for the development of facile and controlled nanodevices.

Contributing more to patterning growth techniques, (L. Li et al., 2009) proposed a method to grow ultralong nanowires with honeycomb-like micro patterns. This method was realized by a reaction of zinc foil with aqueous $Na_2C_2O_4$ as shown in detail in Figure 2.4. Their photosensitivity was found to be about 10 at 5V. After the characterization of
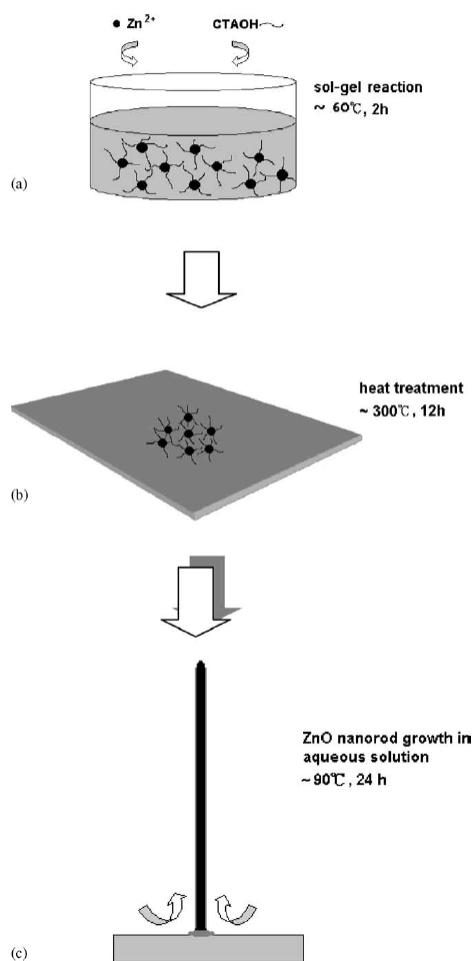
Figure 2.1: The soft chemical method used on the glass substrate. (a) and (b) describes the sol-gel reaction and the dispersion on substrate. (c) describes the growth of ZnO nanorods through hydrolysis-condensation process. (Hung & Whang, 2003)
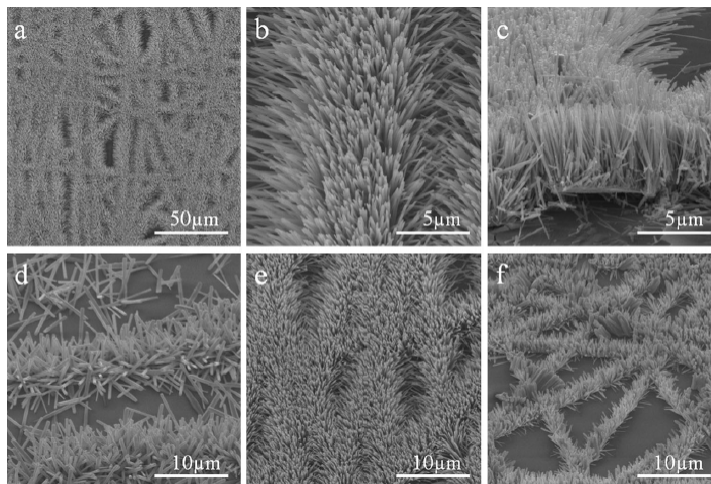
Figure 2.2: Different nanowire growth for fibers calcined at different temperatures and varied amount of time. (Liu et al., 2016)
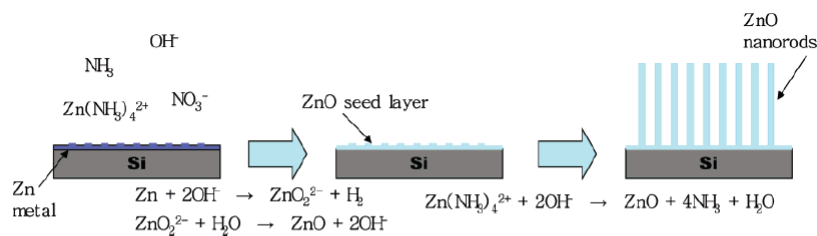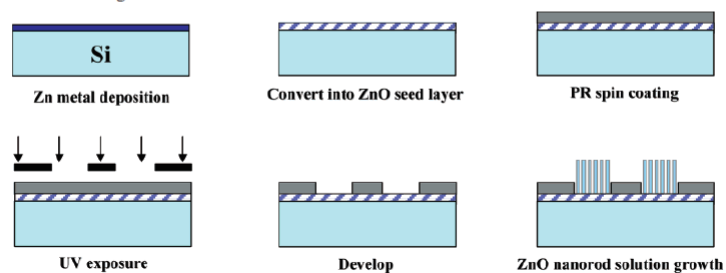
Figure 2.3: Proposed Procedure by (Tak & Yong, 2005)

various parameters, it is concluded that these nanowires are ideal as chemical sensors or photoelectronic devices.

Literature suggests, various seeding techniques are used in each hydro-thermal method. Some authors compared the resulting nanorods via two or more seeding techniques. One
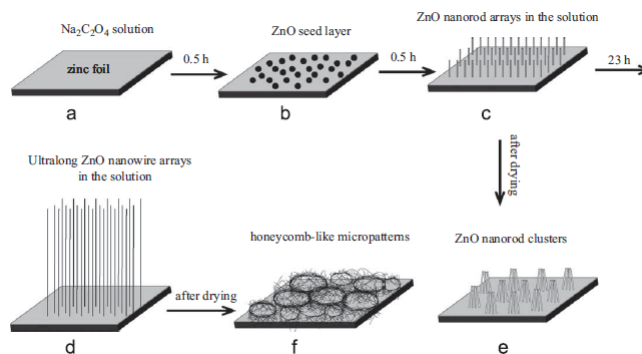
Figure 2.4: Procedure for formation of micropatterned arrays of ultralong ZnO nanowires (L. Li et al., 2009)

such study was carried out by (Dong et al., 2013) comparing results of dip coating and radio frequency magnetron sputtering on a Silicon substrate. It was found that, RF magnetron sputtering, dip coating results in larger size distribution and surface roughness of the seed layer. Also, the nanorods aligned perfectly normal to the substrate with uniform length in the sputtering method proving that this method has a clear advantage. However, this method is expensive and has a wide range of limitations on substrate size. Thus, in the current research, dip coating is employed.

All the studies above described various methods for the growth of ZnO nanorods. There are also investigators that summarized various morphologies of ZnO being produced in the hydrothermal procedure. (Pal & Santiago, 2005) categorized various morphologies of ZnO nanorods based on the pH of the growth solution as shown in Table 2.1. The constituents of the aqueous solution were water, ethylenediamine (En), zinc acetate dihydrate and sodium hydroxide in various proportions. In this context, it is apt to mention a model developed by (Demes et al., 2016) which describes the nanowire growth in relation to seed layer properties and growth duration. Mean grain size (MGS), surface coverage rate (SCR),

and texture coefficients of the sol-gel procedure via grown ZnO nanowires are varied, in addition to various combinations of growth time and multilayer procedures to vary film thickness (Table 2.2). Equations to determine the diameter and length of the nanowires were formulated with some valid assumptions. The initial diameter of the nanowires were found to be 20 nm with approximate longitudinal and lateral growth rates of 25-30 nm/min and 0.01 nm/min, respectively.

Table 2.1: Change in morphology of ZnO nanostructures with various parameters (Pal & Santiago, 2005)

sample	En	pH_i	pH_f	morphology
ZnO-1	10%	8.6	11.0	elongated nanoparticles
ZnO-2	10%	9.0	11.0	flower like nanostructures
ZnO-3	10%	10.0	11.0	inhomogeneous nanorods
ZnO-4	10%	10.0	12.0	inhomogeneous nanorods
ZnO-5	10%	11.0	12.0	homogeneous nanorods of high aspect ratio
ZnO-6	5%	8.6	11.0	inhomogeneous nanorods
ZnO-7	5%	9.0	12.0	homogeneous nanorod bundles
ZnO-8	5%	10.0	12.0	homogeneous nanorods with low aspect ratio
ZnO-10	5%	8.6	12.0	defective nanoparticles, short nanorods, and rectangular nano-sheets

Table 2.2: Summary of various combinations of specimen (Demes et al., 2016)

Samples	ZnO seed layer			ZnO nanowire			
	SCR (%)	MGS (nm)	Texture coefficient (%)	NW apparent length (μm)	NW mean diameter (nm)	NW aspect ratio (a.u.)	NW surface density (μm^{-2})
a1	88	40	80	2.6	83	31.3	44
a2	99	40	80	2.5	82	30.5	38
b1	99	36	55	2.8	78	35.9	30
b2	99	57	55	3.1	99	31.3	18
c1	98	48	54	2.8	86	32.6	26
c2	98	48	100	2.5	81	30.9	49

Moving more towards the chemistry involved in the hydrothermal process, dispersions of various metal oxides nanowires and nanoparticles in different solvents was studied by

Ghosh et al. (Ghosh et al., 2009). The nanowires of ZnO, Fe_3O_4, and TiO_2 were dispersed in water, dimethylformamide (DMF) and toluene separately in the presence of various different combinations of surfactants. In the particular case of ZnO, which is of great significance in the current research, polyethylene oxide (PEO), sodium dodecyl sulphate (SDS) and sodium bis (2-ethylhexyl) sulphosuccinate (AOT) in water, AOT, polyethylene glycol (PEG), polyvinyl alcohol (PVA), PEO and Triton X-100 (TX-100) in DMF, PEO in toluene were found be the best surfactant-solvent combinations. Weak non-covalent interactions were formed with the nanostructures by the surfactants keeping their physical properties intact.

Various inverstigators worked on a wide range of hydro-thermal methods as described above. Some of them along with various parametric analysis are described in the following works. (Akgun et al., 2012) synthesized ZnO nanowires using zinc acetate dihydrate as a zinc salt as opposed to commonly used salts like zinc nitrate hexahydrate, zinc acetate, and zinc chloride. The effects of parameters like time, temperature, solution concentration and concentration ratios of the precursor chemicals on the growth were studied.It was concluded that the diameter of the nanowires depend on the concentration of the precursor chemicals while their length is more likely to depend on the temperature and time involved during their growth. Also, it was observed that this salt eliminates the usage of additional capping agents and results in formation of ZnO nanowires with comparatively less or no impurities.

The next logical step after looking into the seeding and zinc salts is to understand the effects of various chemicals in used in the aqueous bath used for inducing the growth
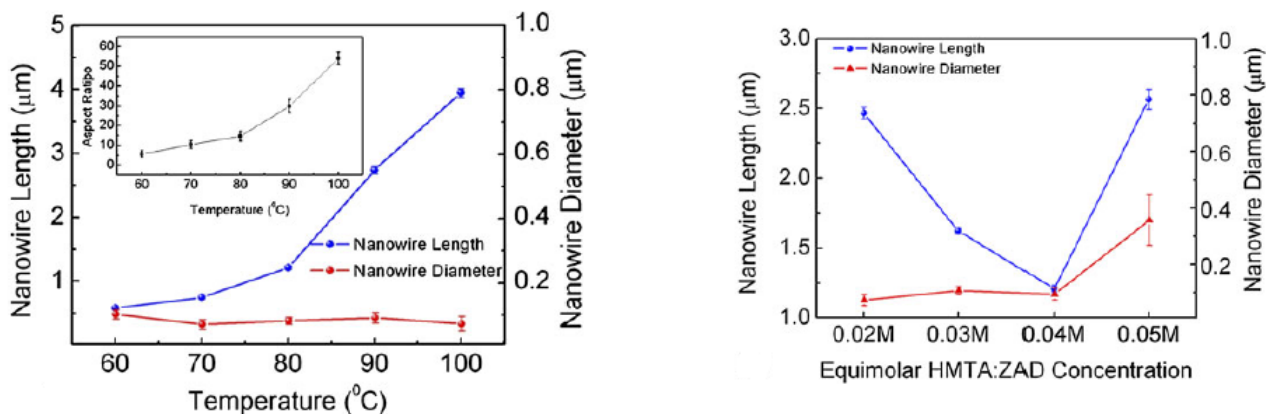
Figure 2.5: The variation of diameter and length of nanowires with various parameters
(Akgun et al., 2012)

of nanorods. Though each chemical has its own significance, hexamethylenetetramine

(HMTA) is worth mentioning due to the role it plays. (Strano et al., 2014) explained the

dual role of HMTA in the growth of ZnO nanorods in chemical bath deposition growth

method. It was noticed that in the presence of less HMTA, the ZnO nanorods structures

were not to be seen, confirming that HMTA bias growth along c-axis and ensures vertical

alignment. This was achieved through a steric hindrance effect which results in inhibition

of lateral growth. Also, it is a well known, pH regulator. Thus, this study highlights the

clear advantages of HMTA in a hydrothermal growth process.

3. Synthesis

This section details the various experimental trials carried out for growing ZnO nanorods on carbon fibers. The IM7 carbon fiber manufactured by Hexcel company was used throughout. As mentioned in the previous section, there is an abundant research available for the growth of ZnO as such on flat substrates like silicon and glass. But there are very few who tried the same on woven fiber surface. This has proven a challenge which led to the prolonged parametric method employed throughout this research. Before achieving a valid synthesis, there are three major steps in this procedure:

3.1   Desizing Step

Every carbon fiber manufacturer adds a protective layer called "sizing" to the fiber for various purposes which include to improve the interfacial properties between fiber and matrix, protect fiber from moisture or aid the processing or production of fiber. A dilute, aqueous liquid consisting of a complex blend of several polymeric components, a coupling agent, a lubricant and a range of additives in water, is coated on fiber in this procedure called sizing. It is necessary for research purposes to remove sizing to expose the true properties of the fiber. Thus, this is the first step called desizing.

Desizing in the current research was carried out by heating the cut fibers to a temperature of 400°C and then cooling down in a span of three hours. The furnace used in this

procedure is as shown in the Figure 3.1 with various components like vacuum pump, nitrogen tank and an electronic console. However, after a few trials, desized fiber was purchased directly from the manufacturer.

Un-sized plain-woven SGP196 (IM7-GP, provided by Hexcel Inc.,) carbon fiber fabric (6 K filaments count in a tow) was used as the main reinforcements.

Figure 3.1: Furnace used for desizing

3.2   Seeding Step

The seeding of the carbon fiber with zinc nano particles is the second step after desizing. There are various methods to do this as described in the literature review. Two methods were tried in this research. They are spray-coating and dip-coating. Spray coating is a technique in which the chemical is loaded to a nozzle from which it is sprayed onto the fibers with a uniform human wrist movement. The thickness of the zinc nanoparticles coated will depend on number of times the chemical was sprayed throughout the fiber. There was one minute time interval between the spraying cycles to allow the sample to dry and prevent agglomeration of ZnO nanoparticles. The chemical solutions tried using this technique were:

Solution 1: 150 mg of ZnO nanoparticles (Nano Tek 40-100nm APS powder, Alfa Aesar) were dispersed in 150 ml of dimethylformamide (DMF) and 1.5 ml of Triton X-100 (TX-100, Alfa Aesar) and homogenized using a Vibra-Cell VCX 500 tip ultrasonic processor for a time of 2 hours at an amplitude of 40%. Then, the mixture was set for 24 hours to stabilize it. Also, after spraying the required amount of layers, the samples are kept at 60° for 24 hours to make sure the complete evaporation of DMF when this chemical solution was used.

Solution 2: Solution 1 was mixed with additional 500 mg of ZnO nanoparticles, 4.5 ml of Triton X-100 and 50ml of water and sonicated using the ultrasonic processor to make a homogenized mixture.

Solution 3: This solution was made by mixing 10 ml of ZnO solution (Zinc Oxide, NanoTek ZN-2551, 50% in H_2O, colloidal dispersion with dispersant 5nm APS for dry powder (typical)-OZn) with 290 ml of water and then homogenizing it with the ultrasonic processor.

The second technique was dip-coating in which the fibers were coated by dipping directly in the chemical solution which was as follows:

Solution 4: 164.6 mg of Zinc acetate was dispersed in 150 ml of Deionised water. 20 ml of ethanol was added to this mixture and then sonicated for 10 minutes to make a homogenized mixture.

This solution was poured into a vessel of large surface area to dip the fibers of a particular cut size. Each time the samples were dipped, they were allowed to dry for 30 seconds and rinsed with ethanol. Finally, after the dipping procedure, the sample was heated at a temperature of 100 °C for 30 minutes.

3.3   Synthesis Step

Once the fibers are coated with zinc nanoparticles, there are certain conditions like temperature, catalysts, pH regulator, etc., which provoke their further growth into nanorods. A chemical bath is prepared using zinc acetate dihydrate ($Zn(O_2CCH_3)_2 2H_2O$) (ZCD), hexamethylenetetramine (HMTA) and deionized water (DI) in certain proportions homogenized thoroughly using the ultrasonic processor. These chemicals were used in different proportions until the best recipe was found. The fibers were immersed in this aqueous solution and placed inside the furnace at a particular temperature for a certain amount of time

to grow the nanorods. So the varying parameters were the time, temperature and concentration of the chemicals. Finally, the density of the nanorod growth, their length and diameter are observed under the Scanning Electron Microscope (SEM).

The various experiments performed and their results are summarized in the following tables and figures:

Table 3.1: Variations in the seeding methods, substrates, and layers through various trials

Trial No.	Seeding Technique	Seeding Solution	No. of layers	Substrate
1	Spray coating	Solution 1	5	Carbon fiber(CF)
2	Spray coating	Solution 1	5,7,10	CF
3	Spray coating	Solution 2	5	CF
4	Spray coating	Solution 3	5	CF
5	Spray coating	Solution 3	5,8,10	CF
6	Spray coating	Solution 3	8	CF
7	Spray coating	Solution 3	8	CF
8	Dip coating	Solution 4	5	Silicon wafer
9	Spray and dip	Solutions 2,3,4	5	CF,Silicon wafer
10	Dip coating	Solution 4	5	CF
11	Dip coating	Solution 4	5	CF
12	Dip coating	Solution 4	10	Graphene Sheet
13	Dip coating	Solution 4	5	CF
14	Dip coating	Solution 4	10	Desized CF
15	Dip coating	Solution 4	5	Desized CF
16	Dip coating	Solution 4	10	Buckypaper
17	Dip coating	Solution 4	5	Buckypaper

Table 3.2: Variations of chemical concentrations, temperature and time through various trials

Trial No.	ZCD (mg)	HMTA (mg)	Water (ml)	Temperature (°C)	Time (hrs)
1	1310	841.08	Distilled 300	83	8
2	2620	1682.16	Distilled 600	83	8
3	2620	1682.16	Distilled 600	83	8
4	2620	1682.16	Distilled 600	83	8
5	5240	3364	Distilled 600	83	6
6	5240	3364	Deionized(DI) 600	83	6
7	2634	1682	DI 600	90	8
8	823	525	DI 300	90	8
9	2634	1682	DI 600	90	8
10	2634	1682	DI 600	90	8
11	2634	1682	DI 600	90	8
12	2634	1682	DI 600	90	8
13	2634	1682	DI 600	90	1,2,3,4,6,8
14	2634	1682	DI 600	90	3:30,6
15	2634	1682	DI 600	90	3:30,6
16	2634	1682	DI 600	90	4
17	2634	1682	DI 600	90	4
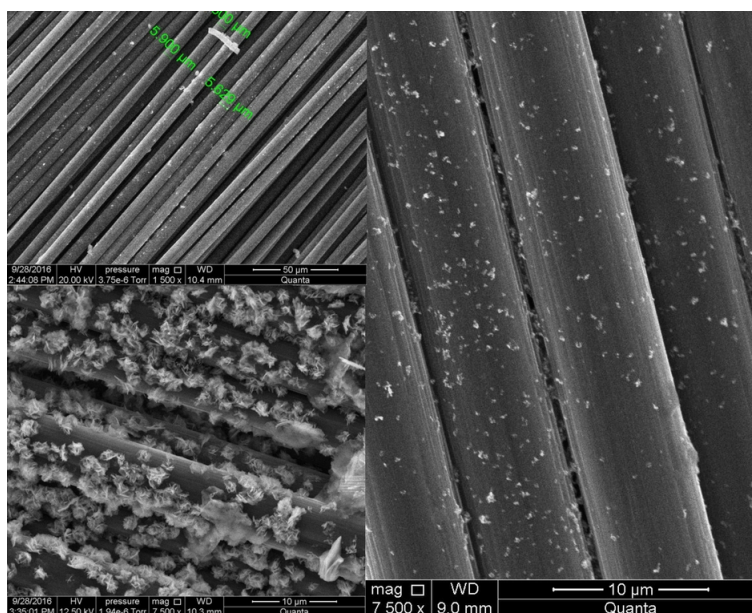
Figure 3.2: Desized fibers, Fibers with Zinc nanoparticle, and Nanoflowers after growth in Trial 1 (clockwise)
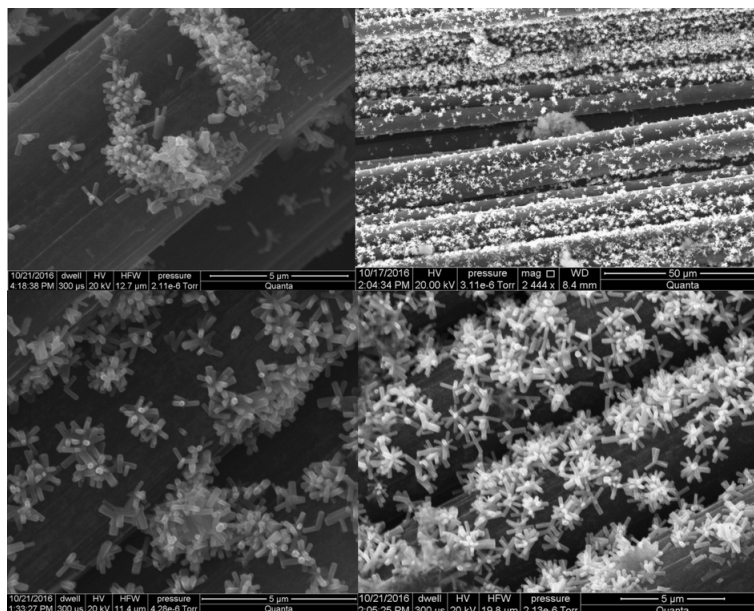
Figure 3.3: Nanorod growth for 7 layers, 5 layers with two magnifications, and 10 layers for Trial 2 (clockwise)
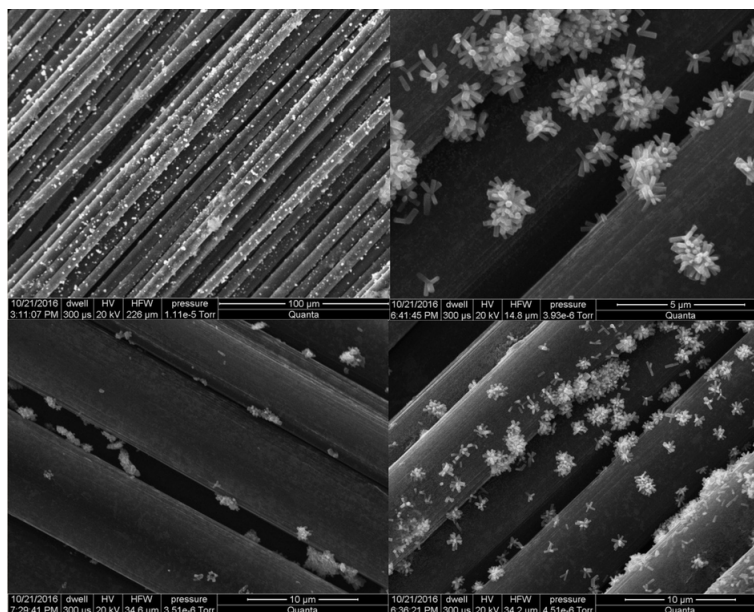
Figure 3.4: Nanorod growth for 5 layers at different magnifications, sparse growth on the bottom side of CF in Trial 3 (clockwise)
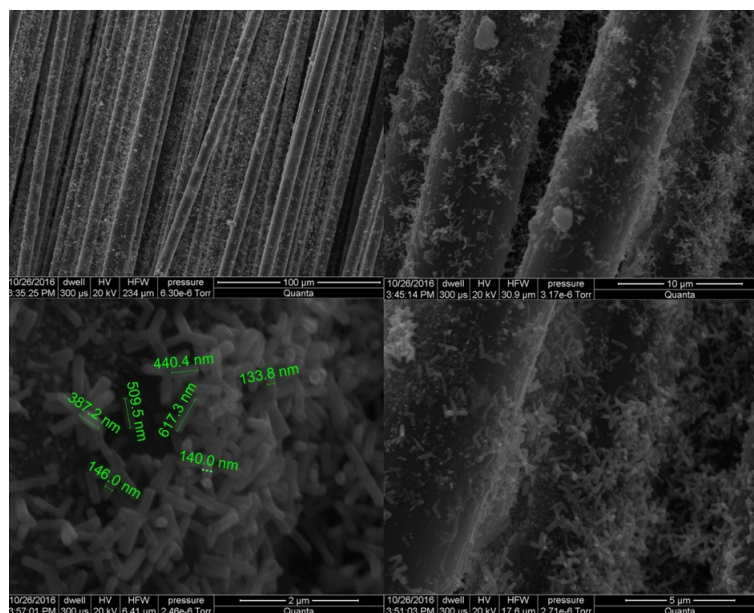
Figure 3.5: Nanorod growth at different magnifications for Trial 4
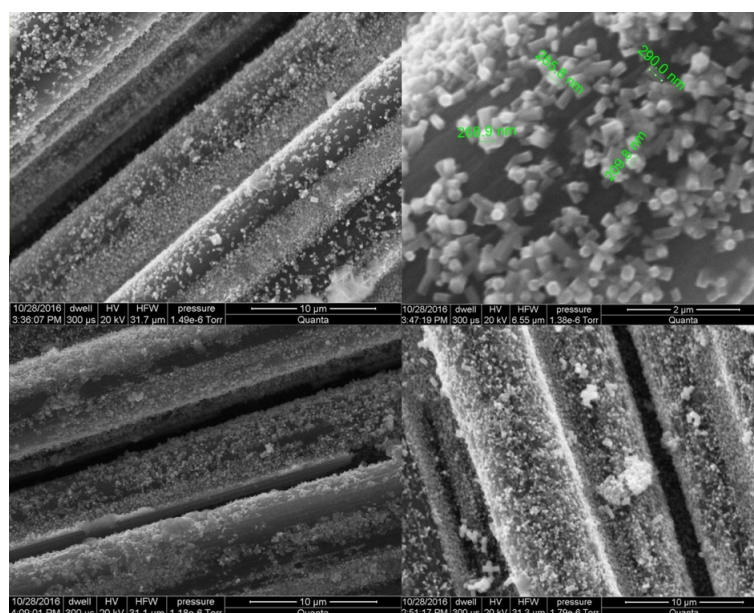
Figure 3.6: Nanorod growth for 5 layers at two magnifications, 8 layers and 10 layers in Trial 5 (clockwise)
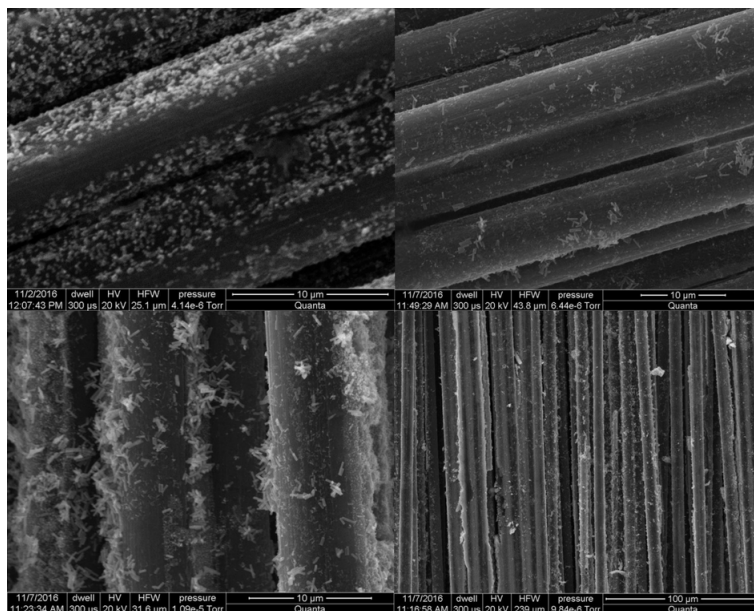
Figure 3.7: Nanorod growth for 8 layers in Trial 6, Sparse growth on the bottom side and nanorod growth at different magnifications on top side in Trial 7 (clockwise)
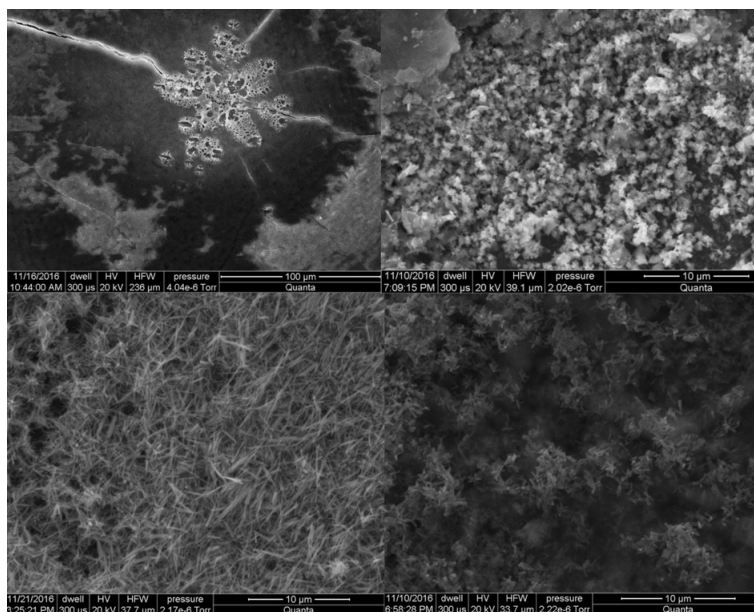
Figure 3.8: Nanorods burnt into silicon, growth on bottom side and top side in Trial 8, Wild nanorod growth on silicon in Trial 9 (clockwise)
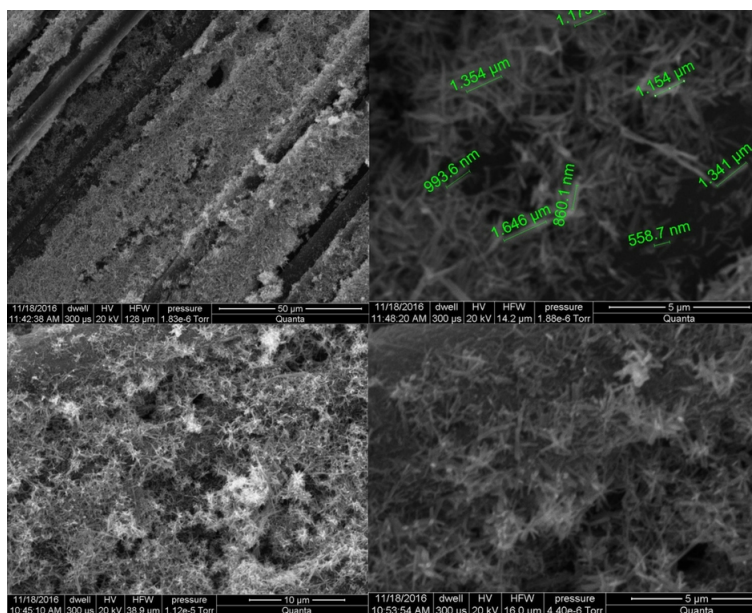
Figure 3.9: Growth using solution 2 in two magnifications, growth using solution 3 in two magnifications in Trial 9 (clockwise)
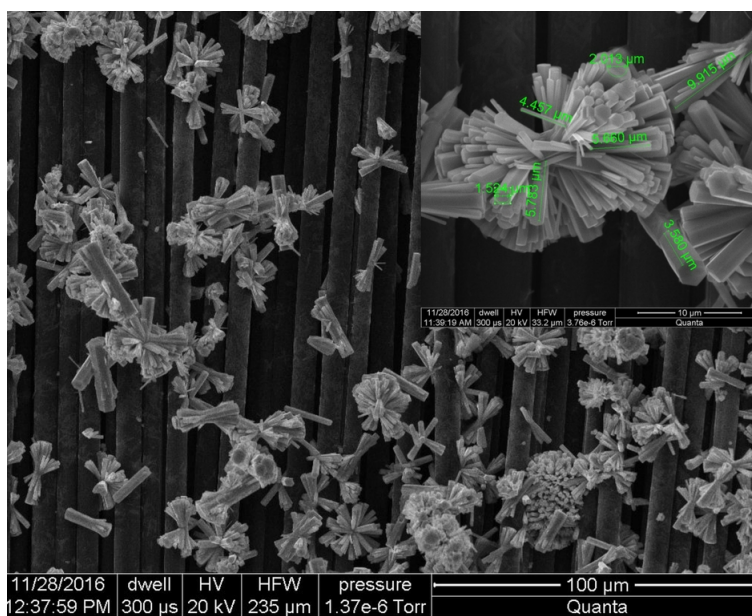
Figure 3.10: Too long dispersion of carbon fiber in growth solution due to a faulty furnace resulting in long and entangled nanorods in Trial 10
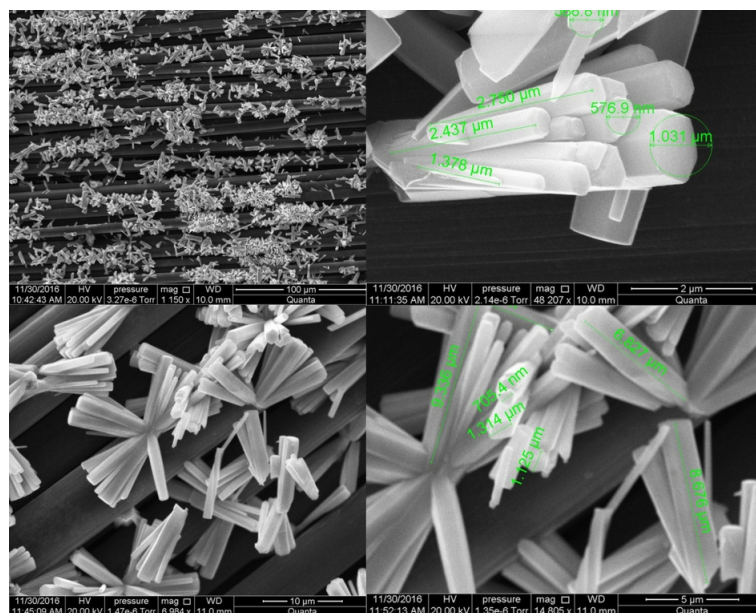
Figure 3.11: Top side nanorod growth on CF at two magnifications, bottom side growth on CF at two magnifications in Trial 11 (clockwise)
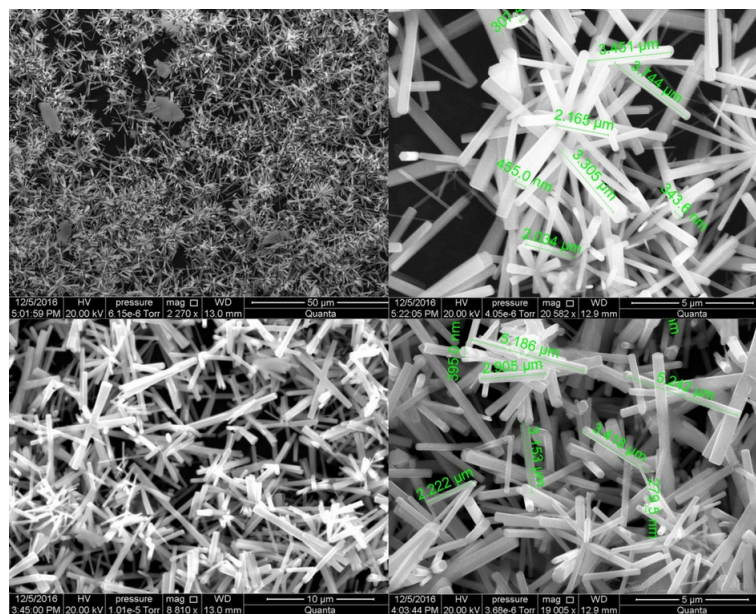
Figure 3.12: Bottom side growth of nanorods on graphene sheet in two magnifications, Top side growth of nanorods on same graphene sheet in two magnifications as explained in Trial 12 (clockwise)
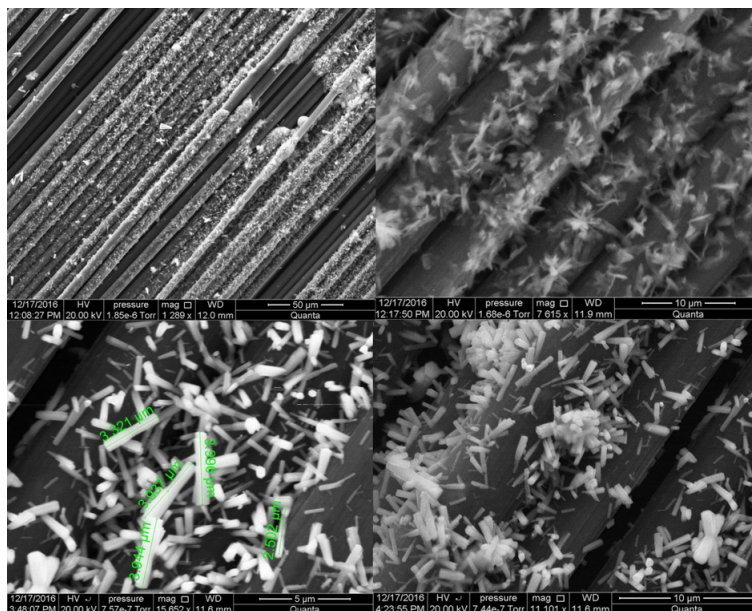
Figure 3.13: The nanorod growth at two magnifications after 1 hour growth, and after 2 hours growth at two different magnifications in Trial 13 (clockwise)
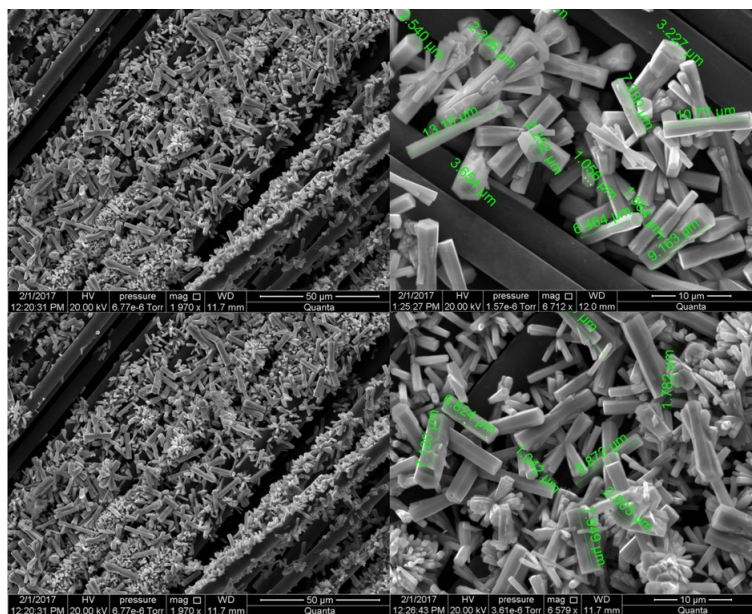
Figure 3.14: Nanorod growth after 3:30 hours(two magnifications) and after 6 hours growth (two magnifications) in Trial 14 (clockwise)
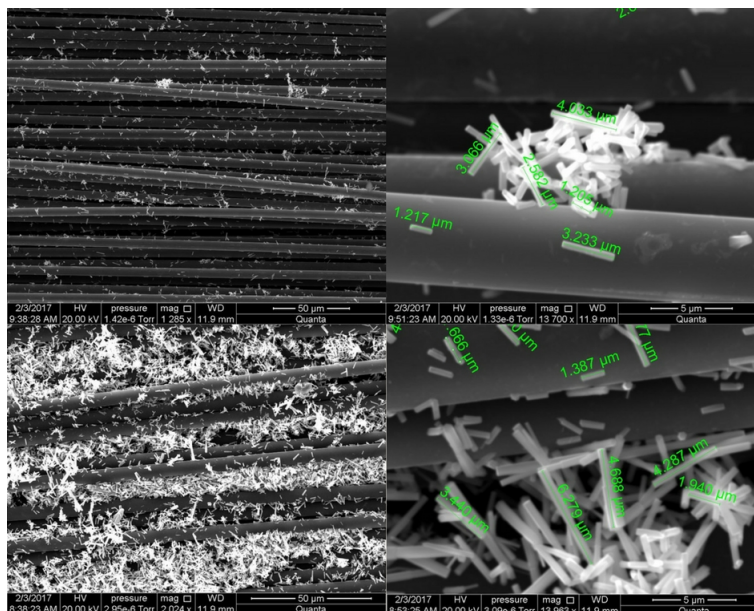
Figure 3.15: Nanorod growth after 3:30 hours(two magnifications) and after 6 hours growth (two magnifications) in Trial 15 (clockwise)
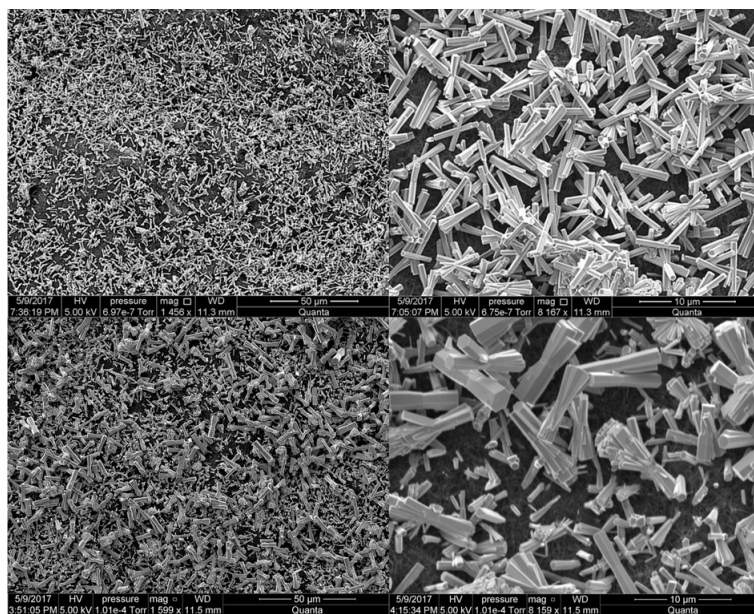
Figure 3.16: Nanorod growth after 4 hours, 10 coatings(two magnifications) and after 4 hours, 5 coatings (two magnifications) in Trial 16 and 17 on Buckypaper (clockwise)

3.4   Summary

To summarize, the first seven trials were attempted with spray coating technique with varying number of coatings of seeding solution from five to ten. Also, in these trials, the best method and time to dry the sample was established. Distilled water was replaced by deionized (DI) water in the 6th trial for better results. The concentrations of HMTA and Zinc Acetate were doubled in 5th trial to look at the variation in growth it causes. The results for growth were still not good enough. Growth was sparse and not uniformly distributed across the fiber.

Eighth trial was carried out on silicon wafer as it has a flat surface to easily comprehend the results. A new method for seeding called dipping was used. Also , a different growth solution was utilized.

In the ninth trial, samples were tested with all dipping solutions, and techniques, and same growth solution on carbon fiber but with one major difference. During the growth stage when the sample was immersed in the solution was placed in the furnace, it was covered with aluminum foil to prevent evaporation during the process.

It was also observed in the above trials that the growth was sparse on the bottom layer of carbon fiber due to the way it was being placed inside the furnace in the growth solution (initially placed face down). This was rectified by using aluminum placeholders to mount the carbon fiber inside the container when placing it in the furnace.

The next trials till the number 15 were made to establish the best growth time for the nano-rods with the required size for our application. This is done by varying the number of

times the fiber is dipped in the seeding solution and also performing the growth on various samples in intervals of 1 hr, 3 hr, 6 hr and 8 hr and finally, observing the growth under SEM. Also, one experiment was done to observe the growth on graphene sheet. Finally, it was established that solution 4 using dipping technique, five layers, and six hours in the furnace at 90°C yields best results.

4. Composite Preparation and Characterization

The plane woven carbon fibers of equal dimensions were cut based on the number of layers required. ZnO nanotubes were grown as explained in the previous chapter. Else they were used unprocessed after drying in oven at 90°C to remove any accumulated moisture. Following the fibers, epoxy accounting to 60% of the weight of the fibers was formulated. The hardener (Aeropoxy, PH3665) and resin (Aeropoxy, PR2032) were blended in 1:4 ratio for the purpose. Simultaneously, aluminum plate and vacuum bag were assembled to house the fibers inside the composite press machine (Wabash MPI). The fibers were then mounted on this assembly by rolling epoxy in between layers in a uniform fashion. The breather cloth is then placed on the top followed by a cover up using vacuum bag. This assembly is then positioned inside the press and connected to a vacuum pump. This setup was achieved to eliminate any epoxy leakages or voids due to the presence of air. The machine was programmed to maintain a pressure of (0.8 Torr) at 60°C for two hours. Later the composite was cured for 24 hours at room temperature.

To proceed with the tensile testing process after fabricating the composite, it was necessary to attach tabs and the cut the composite plates to a minimum of 10 samples. Tabs provide the necessary friction to hold the composite strip in the flat hydraulic grips of the tensile testing machine. These were made of fiber glass in this research. They were machined to have rough surfaces and tapered edges for better adhesion. Epoxy, in the similar

ratio as before (1:4 hardener to resin) was used as an adhesive. The assembly of the composite plate and tabs was allowed to cure for 24 hours before it was cut into strips of half inch width in the machine shop using cutting saw in the machine shop.

Five configurations of two layer composites were made for this experiment: One with just carbon fiber as is, no Bucky paper, no ZnO (CF as is, no BP), second with carbon fiber, and nanorods on bucky paper (CF as is, ZnO on BP), third with ZnO nanorods on carbon fiber, no Bucky paper (ZnO on CF, no BP), fourth with nanorods on carbon fiber, Bucky paper as is (ZnO on CF, BP as is), fifth with both carbon fiber and Bucky paper as is (CF and BP as is). Initially, tensile test was performed followed by fracture, DMA and resistivity analysis.

4.1 Analysis

4.1.1 Tensile Testing

The samples were ready to be analyzed after the positioning of tabs. Each sample was the size of 5" × 1/2". The tensile tests were carried out following the ASTM-D3039/D3039M-08 standard (*Standard Test Method for Tensile Properties of Polymer Matrix Composite Materials*, 1995), utilizing a Tinius Olsen testing frame (Model 150ST) under 1.0 mm/min constant crosshead speed. A Tinius Olsen extensometer with 1 inch gauge length was used to record the strain. The stress vs. strain data for different test coupons were recorded and analyzed in order to report the samples elastic modulus, ultimate strength and strain

to failure. A minimum of 12 samples were tested for each configuration. The results were exported and analyzed in Microsoft Excel.

4.1.2 Fracture Analysis

After tensile testing, the fractured surface are handled with utmost care and mounted on the Scanning Electron Microscope (SEM) sample holder. This is a highly advanced technique in the field of microscopy used for magnifications inaccessible by light microscopes. In simple terms, SEM uses electrons from a focused electron beam to scan the sample back and forth which results in the formation of an image. These images are called micrographs. The electron beam, when interacted with the sample emits a multitude of signals like secondary electrons, backscattered electrons, X-Rays, cathodoluminescence, and auger electrons. However, only secondary electrons and backscattered electrons are used in common for imaging purposes.
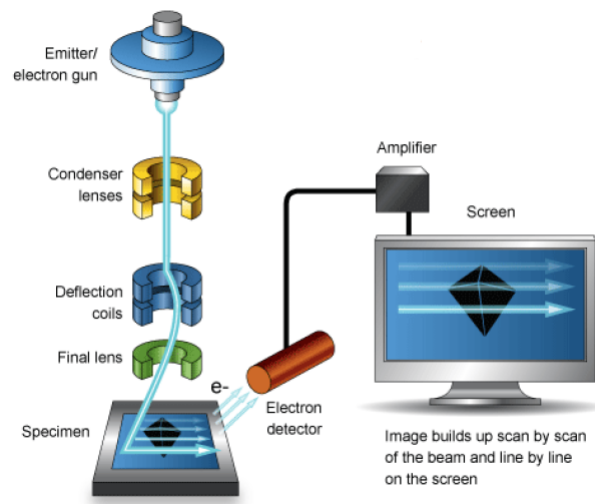
Figure 4.1: Various parts and working of SEM (*Scanning Electron Microscope Training Module*, n.d.)

Figure 4.2: Fracture in Samples

Figure 4.3: Delamination and fracture surfaces

FEI Quanta 650 SEM was operated in a High vacuum mode with a tungsten thermionic gun for emitting electron beams, in this research. Also, secondary electron detector (Everhart-Thornley Detector), with a positive bias to attract low energy secondary electrons was used for forming micrographs. Due to the low atomic number of the specimen, various problems arose in imaging at high magnifications. Thus, gold coating, proper accelerating voltage and ideal spot size for the current were various factors which decided the quality of the topographical information acquired. In fracture analysis, for each composite configuration, sample with high proximity to the average strength of a particular configuration was chosen. The sample was examined for the presence of fiber or matrix failure and possible defects in nanorods. Micrographs at various magnifications were captured.

4.1.3   Dynamic Mechanical Analysis (DMA)

This test is used to find the damping and stiffness of a given sample during the application of a sinusoidal force. The quantities being measured for the purpose are tan (δ), storage modulus and loss modulus. The storage modulus, E is the measure of sample's elastic nature. Tan (δ) is the ratio of loss to storage moduli. In addition, this method is also used to find the glass transition temperature of a material.

In the current research, PerkinElmer Dynamic Mechanical Analyzer, DMA 8000 was used. The DMA tests were carried out utilizing the following the ASTM D4056-06 standard. Samples of size (44.5 $\times$ 6.4 $\times$ 1.6 mm) were cut accordingly. Dual cantilever technique is used to mount each of them on the machine. This is followed by temperature and frequency sweep tests being performed on that sample. In the former test, a constant frequency of $1Hz$ is applied, with variation in temperature from $30^{\circ}C$ to $160^{\circ}C$ at a constant force and strain of $2N$ and $0.03mm$ respectively. The glass transition temperature was observed from the results to estimate the range for frequency analysis. Once the range was established, the latter test was performed with a frequency variation from $1Hz$ to $200Hz$ scanning over three different temperatures of $30^{\circ}C$, $55^{\circ}C$, and $80^{\circ}C$. The force and strain applied remains constant for both types of tests.

4.1.4   Electrical Resistivity Test

Electrical resistivity is a material property unlike resistance. There are various types of resistivity which include surface resistivity, bulk resistivity and contact resistivity. Though

it is a common practise to measure both surface and bulk resistivity for composites, only surface was possible with the given equipment and time. The samples of each configuration were initially cut into a size following the ASTM standards. Aluminum electrodes using conductive silver epoxy were glued to the samples, followed by curing for 24 hours. The resistance was then measured between the two electrode ends. The sensitivity of the measured resistance was: ($\pm 0.05\%$). Finally, the resistivity was calculated using the formula:

$$(R) \times (L/W) = ohms/square$$

4.2   Characterization of Two Layer Composite Configurations

As mentioned in the introduction, the main aim of thesis was to perform characterization of various hybrid composites. Also, Bucky paper was used as an additional layer in some hybrids. Bucky Shield Grade 100% MWCNT from Buckeye Composites, Inc. comprising MWCNTs with average thickness of 125 micron and density of 0.3-0.4 g/cm^3 was used in the current research . ZnO nanorods were grown on Bucky paper using the identical procedure used for carbon fiber substrate, with the one exception of ten seeding layers instead of five. This number was established by observing the growth for five and ten layers using SEM. Thus, after concluding the synthesis procedures on various substrates, i.e. carbon fiber and Bucky paper, hybrid composites were prepared and analyzed.

4.2.1 Tensile Test

Tensile test was conducted as explained before for each sample. Each configuration had around twelve samples to be analyzed. The data was exported into Excel for each of them after the test. The parameters of interest were strength and stiffness. Thus, calculations were performed accordingly for each sample. Once the strength and stiffness of each sample were calculated, the data was normalized accounting for different volume fractions of fibers in various configurations. Finally, the average parameters of all twelve samples of each configuration was calculated. These results were plotted as shown in Figures 4.5 and 4.6.

Representative stress vs. strain curves for the designed CFRPs, obtained from the tension tests, are illustrated in Figure 4.4. Figures 4.5, and 4.6 show the average values and the standard deviations for the CFRPs tensile strength, and elastic modulus, respectively. The slope of the stress Vs. strain curves of the CFRPs up to the strain value of 0.30% was considered as their elastic moduli. The tensile strength of the designed CFRPs was considered the maximum stress value in the stress Vs. strain data, and the strain to failure to be the strain value at the last data point of the curves.

Figure 4.6 suggests a slight increase 2.0-3.0% in the elastic moduli of the three configurations of CFRPs based on the fibers incorporating ZnO (grown either directly on the fibers or on Bucky paper). Incorporating Bucky paper without functionalizing in between carbon fibers yielded poor results in stiffness as the composite encountered early delamination during the test, which reduced the stiffness by 14%. Functionalized Bucky papers are well-

known for poor impregnation of the epoxy specially in composite fabrication techniques employing pressure (i.e., composite press) Vs. techniques employing vacuum (e.g. autoclave) (Ashrafi et al., 2010). To alleviate this shortcoming some groups utilized carboxyl group functionalization of Bucky paper which yielded structures with more favorable contact angles for epoxy composite processing (Lopes et al., 2010). In this investigation we observed that the growth of ZnO on carbon fiber or on Bucky paper alleviates this delamination by inducing a z-pinning mechanism.

Inferred from Figure 4.4, all the CFRPs showed initial linear-elastic behavior. However, as load increases their behavior deviates from linearity due to initiation of matrix cracking and some individual fiber breakages. The cracks in the matrix could propagate towards the fibers increasing stress intensity close to the fibers causing fiber breakage (more apparent in the CFRPs with no ZnO nanorods; i.e. CF as is with no Bucky paper and CF and BP as is with no ZnO nanorods. Unless the crack is stopped or deflected by the ZnO nanorods forest in the fiber/matrix interface region (such as the CFRPs with surface grown ZnO nanorods and CFRPs with ZnO grown on Buckypaper). In the case of individual fiber breakage, the stress transfer mechanism through the matrix in the fiber / matrix interface region aids the composite to withstand the load. The surface grown ZnO nanorods provide stronger fiber/matrix interface, thereby, help the hybrid CFRPs to resist the failure up to higher strains, and therefore to exhibit more ductile behavior than the CFRPs with no nano-reinforcements as can be seen in Figure 4.4. Hence, the samples with ZnO nanorods (with and without Bucky paper) exhibited enhancements in the strain to failure compared to the reference CFRPs by 27-45%, Figure 4.4.

The strong fiber / matrix region produced by randomly distributed ZnO nanorods in the samples where ZnO was grown directly on the carbon fiber- with no Buckypaper presence- improved the strength of the reference CFRPs by 20%. Growing ZnO on the surface of Buckypaper also yielded 23% improvement of the strength; suggesting that ZnO acts as z-pinning hurdles that assist reducing the delamination of the composite due to poor impregnation of the Bucky paper.

An enhancement of 17% was also shown for a composite where the ZnO grown on the carbon fiber act like an anchoring mechanism for Bucky paper setting on top of the ZnO forests. The only sample exhibited lesser strength than the sample based on raw carbon fiber was the sample incorporating Bucky paper with no ZnO nanorods. As these sample lack the mechanism to resist stress propagation between the matrix and the surface of the Bucky paper (no Z-pinning and no adhesion group between the matrix and the Bucky paper), the stress transfer easily detaching the Bucky paper from the surface of the fibers, leading to local delamination. Delamination failure has a negative effect on the final strength of the FRPs.
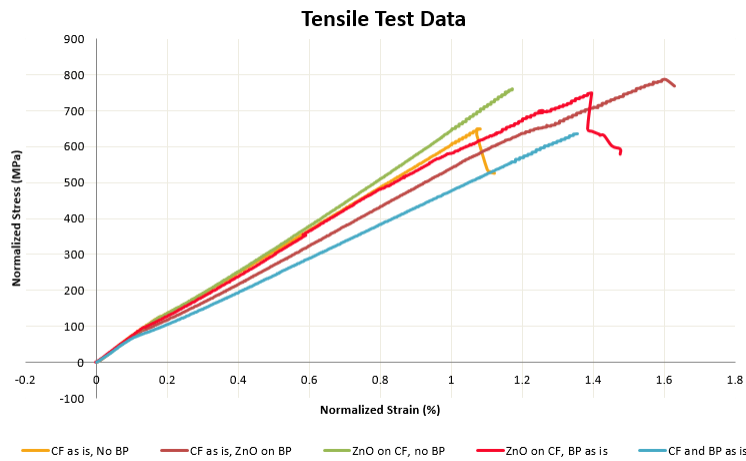
Figure 4.4: Comparison of Tensile Test Data of Various Configurations
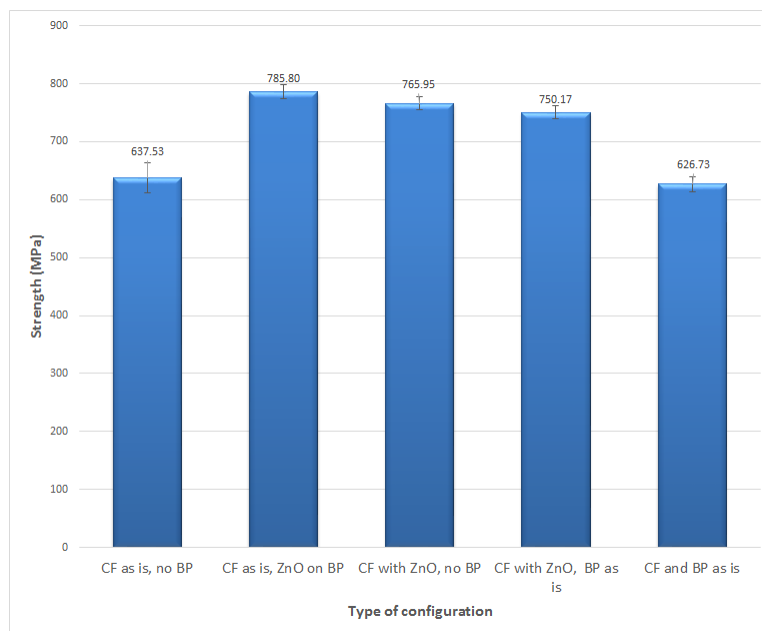
Figure 4.5: Comparison of normalized strength for different configurations
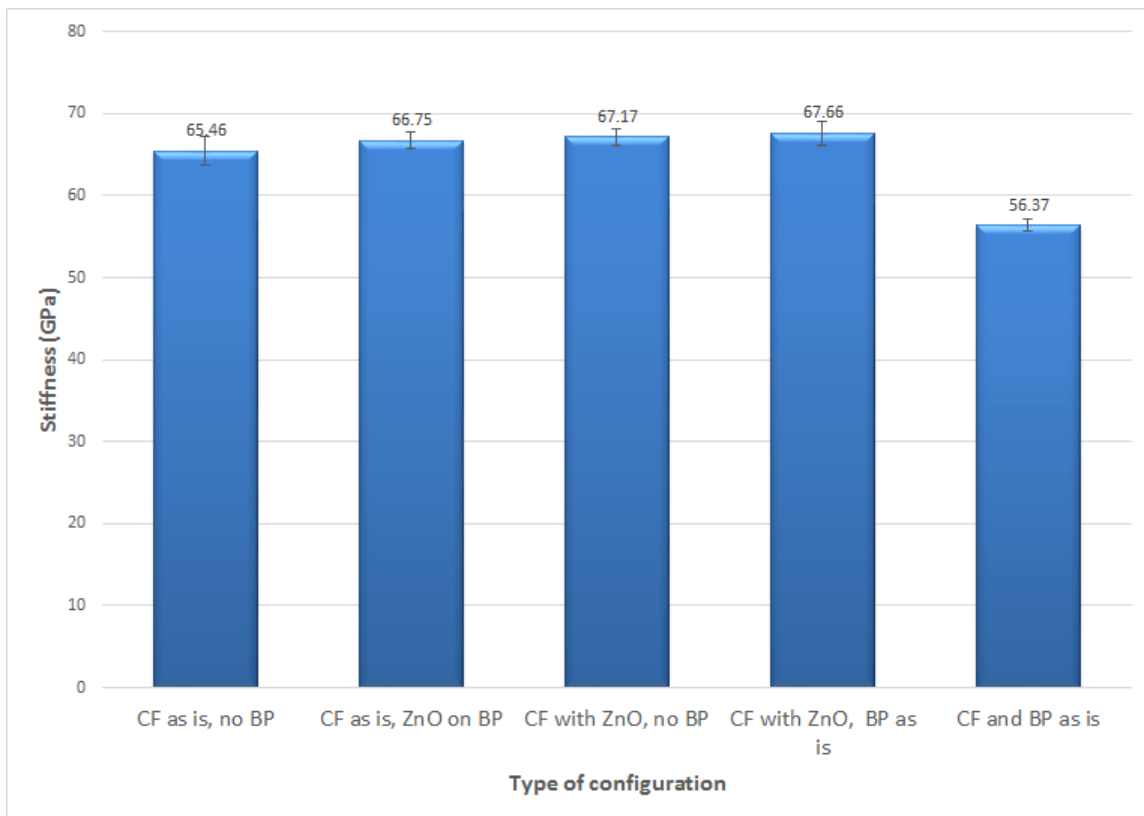
Figure 4.6: Comparison of normalized stiffness for different configurations

Table 4.1: Comparison with respect to the original CF as is , no BP sample

Configuration	% Change in Strength	% Change in Stiffness
CF as is, ZnO on BP	23.26	1.98
ZnO on CF, no BP	20.14	2.61
ZnO on CF, BP as is	17.67	3.36
CF and BP as is	-1.69	-13.88

These figures clearly indicate the increase in strength and stiffness of the hybrid composites due to the growth of ZnO nanorods. Also, it was observed that both stiffness and strength fall drastically in the configuration of carbon fiber (CF) and Bucky paper (BP) as is. This was due to the delamination failure observed in a majority of samples with Bucky paper as the middle layer during the tensile test. The adhesion between carbon fiber and

Bucky paper in hybrid composites should be further investigated to mitigate this type of failure. The highest strength and stiffness were seen in CF as is, ZnO on BP and CF with ZnO, BP as is respectively.

The sample with the nearest average strength in each configuration was selected to plot the graph as shown in Figure 4.4. The data was normalized by volume fraction before plotting to ensure valid comparison. This compares the elastic behaviour of various hybrid composites. The highest and least slopes were seen in the hybrid composite with ZnO on CF, no BP, and CF and BP as is respectively. Again, the effects of delamination were confirmed.

4.2.2   Fracture Analysis Using SEM

After the tensile test was performed following the ASTM standards, fracture analysis using SEM was followed. The sample with strength closer the average strength of the respective configuration was chosen for analysis in each case. Once the sample was chosen, the area where the tensile test failure occurred was carefully severed and mounted under the SEM. In the case of delaminated samples, both split surfaces were analyzed to get a comprehensive idea of how failure occurred. The results are as shown in the following micrographs:

Figure 4.7: Fracture analysis of the configuration with just CF and no BP

Considering Figure 4.7 clockwise, the first micrograph shows both matrix and fiber failure at a higher magnification. The second one shows broken and mis-aligned fibers at a lower magnification. The third one shows just matrix failure for a very lower magnification. The last one shows broken fibers at different layers. Thus, it can be concluded this composite, made just out of carbon fiber experienced both matrix and fiber failure.
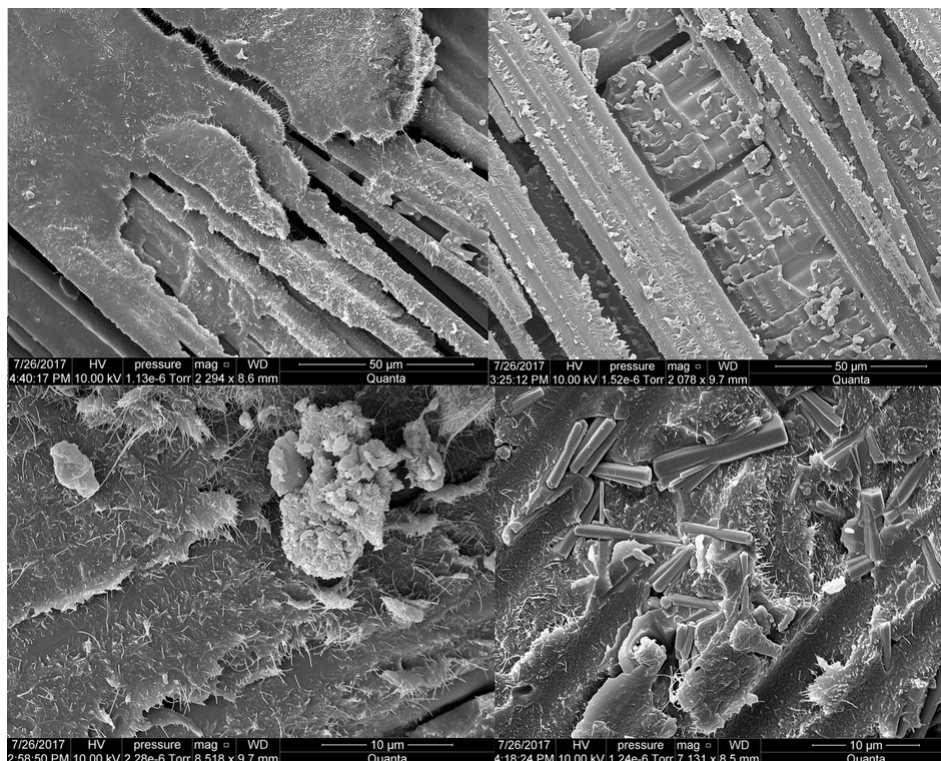
Figure 4.8: Fracture analysis of the configuration with just CF and ZnO on BP

Considering Figure 4.8 clockwise, the first micrograph shows the failure along matrix while the fibers seemed intact. The second one shows mis-oriented fibers at various layers. The third one shows the nanorods on Bucky paper entangled with fibers. The last one shows the Bucky paper on fibers at higher magnification. Thus, it can be concluded that the failure predominantly was along the matrix.
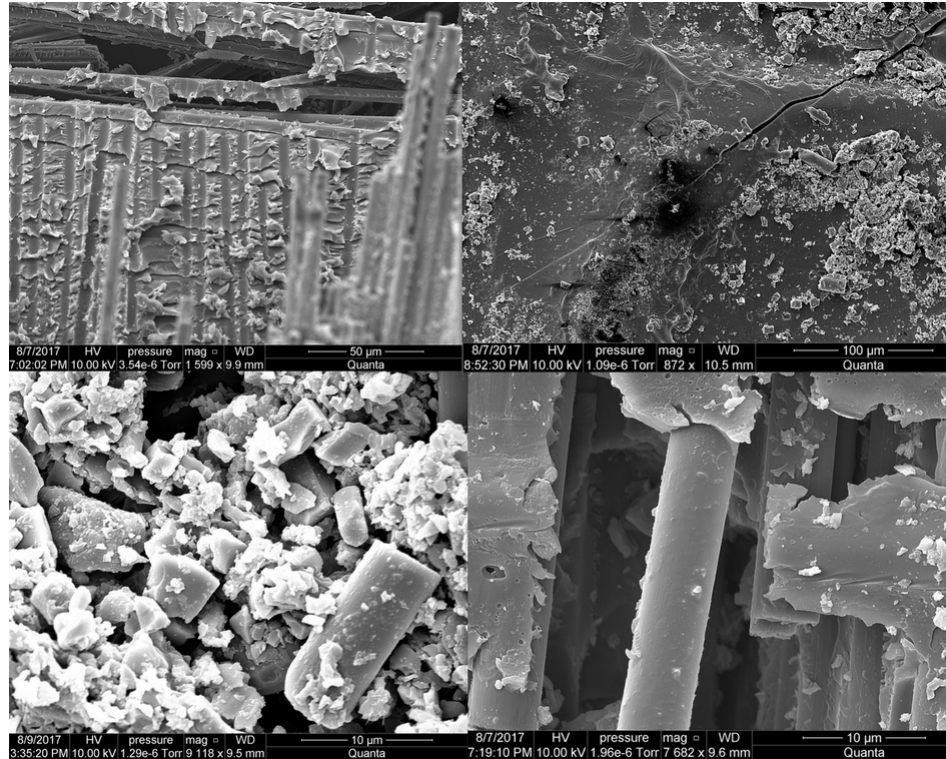
Figure 4.9: Fracture analysis of the configuration with ZnO on CF and no BP

Considering Figure 4.9 clockwise, the first micrograph shows split fibers between different layers. The second one shows an extended crack along the matrix. The third one shows the void the matrix failure leaved behind between fibers. The fourth one shows a cluster of nanrods.Thus, it is safe to conclude that, the failure predominantly was along the matrix.
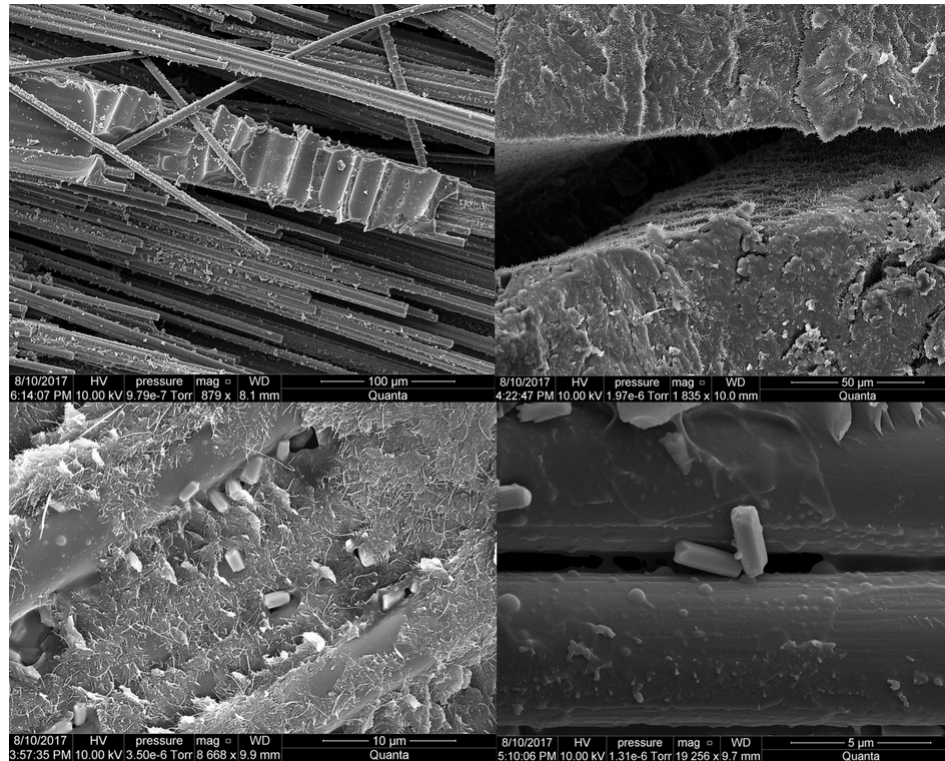
Figure 4.10: Fracture analysis of the configuration with ZnO on CF, BP as is

Considering Figure 4.10 clockwise, the first micrograph shows the haphazardly oriented fibers with a clear matrix failure. The second one shows the Bucky paper split along the matrix. The third one shows the ZnO nanorods on the fibers. The last one shows the bucky, ZnO nanrods and fibers entangled together. Thus, even in this hybrid composite, it can be concluded that the failure is predominantly along the matrix.
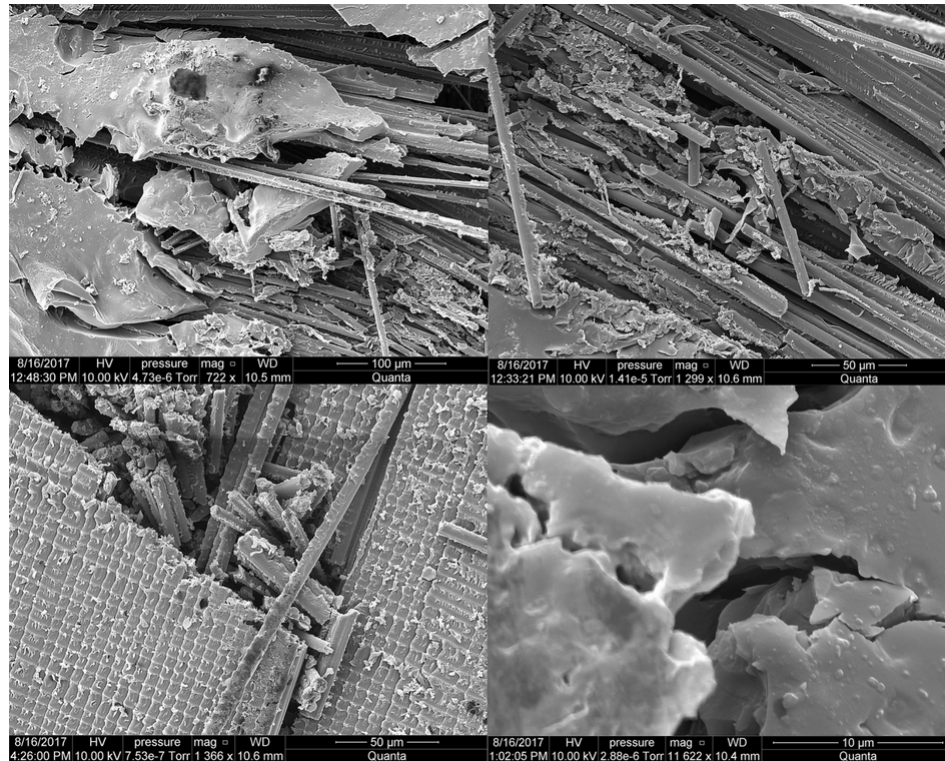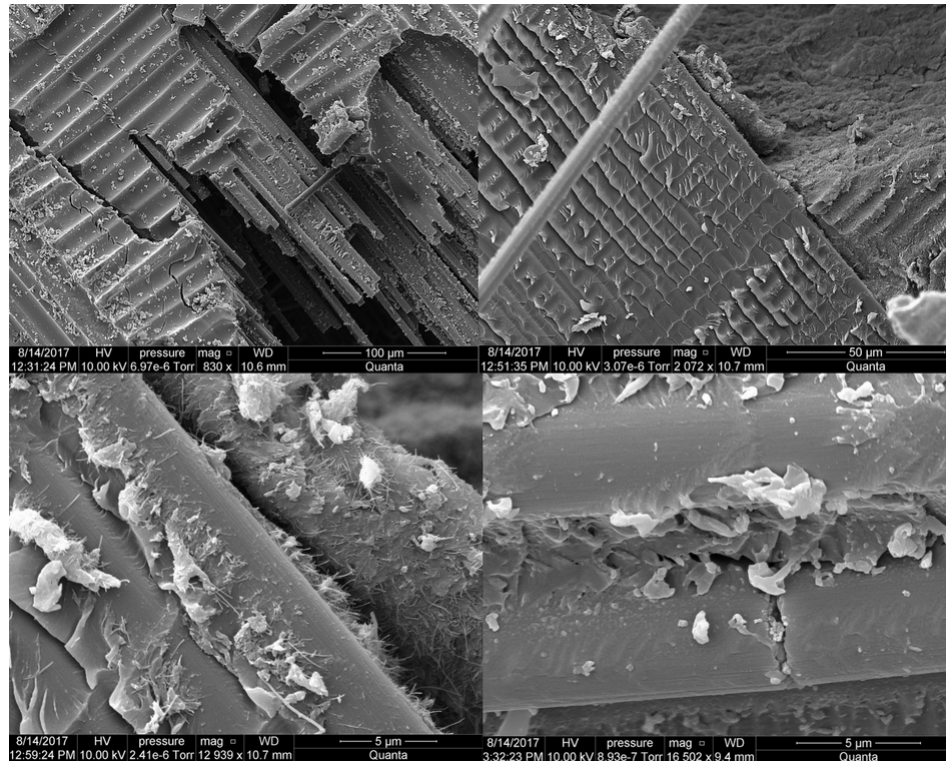
Figure 4.11: Fracture analysis of the configuration with CF and BP as is

Considering Figure 4.11 clockwise, the first micrograph shows the failure along the matrix with continuous fibers running through the middle. The second one shows the interface of Bucky paper, carbon fiber and the matrix. The third one shows the fiber fracture. The last one shows the Bucky and fiber interface. Thus, this hybrid composite failed along both matrix and fiber.

Thus, the fracture analysis of all the hybrid composites concludes that the presence of nanorods reduce the chances of failure along the fiber, thus increasing the overall strength and stiffness of the structure. Bucky paper, though split due to delamination, remained continuous throughout. Thus, if the adhesion between various layers was better, the parameters of interest will be enhanced.

4.2.3 DMA Analysis

The samples for DMA analysis were cut before the tensile testing. This was to prevent any discrepancies which may appear in the results. One sample of each configuration was tested. As stated before, both temperature and frequency scans were carried out. The results were analyzed from the following graphs:

Temperature Scan Graphs

Figure 4.12: Graph showing the variation of tan delta with temperature for various configurations of two layer composite samples

The thermal DMA curves are depicted in Figure 4.12 showing variation of the loss tangent; tan (δ) with temperature. Three composites configuration seem to attain peak values of tan (δ) at an identical glass to rubber transition temperature (T_g) close to 78°C; namely the composites based on raw fibers, or based on fibers with surface grown ZnO and

sample with ZnO grown over Bucky paper. The two other configurations of carbon fiber and Bucky paper; Carbon fiber with ZnO nanorods grown on the surface sandwiched with Bucky paper attained a glass transition temperature closer to 90°C; which is close to the glass transition of the neat epoxy systems as provided by the manufacturer (Tg = 96°C). The reduction of glass transition is indicative of the filler influencing the epoxy cure reaction kinetics. In the present thesis no kinetics studies were performed (due to lack of access to differential scanning calorimetry; DSC system) so it is uncertain if early stage catalysis took place in the case of reaction in the presence of heat-treated composites. However, this thesis is concerned with the product so it is not relevant if minor differences took place in the initial cure mechanism. The final degree of cure is associated with the later stages of the curing process when the molecular weight is such that the mixture exhibits very high viscosity and cure rate is diffusion controlled. In experiences with nano fillers such as CNTs (in the Bucky paper) and ZnO the explanation for a lower degree of cure is ascribed to the fact the presence of nanofillers significantly enhances hindrance to the physical mobility of epoxy active groups and curing agent (Puglia, Valentini, Armentano, & Kenny, 2003), (Tao et al., 2006). In comparison to the composite based on raw fibers tan (δ) exhibited improvement when both ZnO nanorods and the Bucky paper coexisted in the composite. The composite with ZnO grown directly on the Bucky paper attained an increase of 65% in tan (δ) over the composite with no nanofillers. Improvements of 15-28 % were observed for the composites closer to the resin glass transition. The only configuration that exhibited lesser tan(δ), reduced by 9%, is associated with the sample with ZnO grown over the carbon

fiber without Bucky paper. Insufficient drying of the fibers upon growing ZnO is a possible explanation for this behavior.
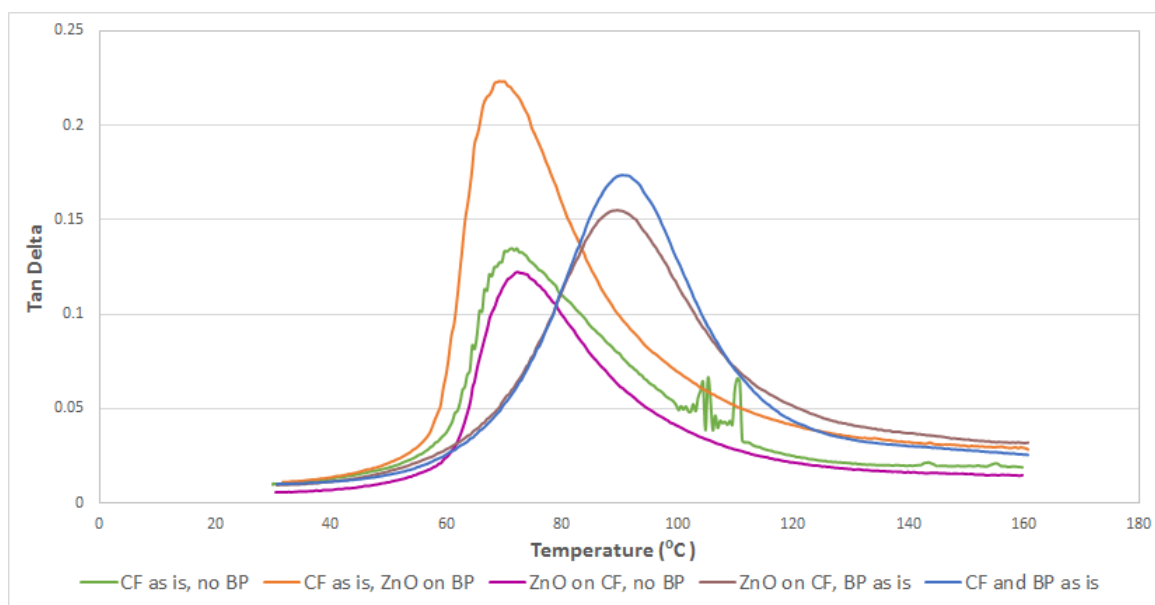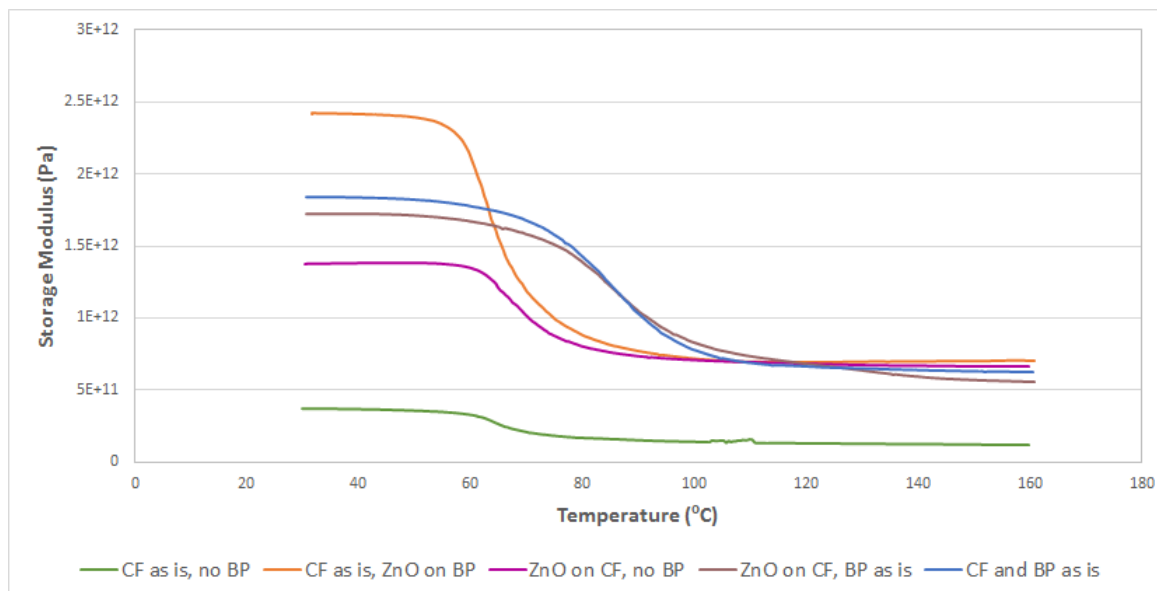

Figure 4.13: Graph showing the variation of storage modulus with temperature for various configurations of two layer composite samples

In the Figure 4.13, the trend of the storage modulus evolution reemphasizes the presence of two sets of composites with two different glass transition temperatures. At room temperature, the trend of the storage modulus is comparable to the tensile stiffness trend; composites with both ZnO and Buckypaper achieve higher stiffness (273-555%) than the composite based on raw fibers. The only exception is for the sample comprising carbon fiber and Bucky paper; as it did not delaminate under the low load of DMA test this sample showed a higher storage modulus than the composite based on the raw fiber while exhibiting lower stiffness in the tensile test due to premature delamination.

As the temperature increases and pass through the glass transition temperature into the rubbery plateau the storage modulus value drop significantly and beyond the glass transition

the difference between the composites with one or more nanofiller is negligible (see Figure 4.13). However, the gap between storage moduli in the rubbery phase temperature range for all the composites with nanofillers are still higher than that for the composite based on raw fibers.

Table 4.2: Comparison with respect to the original CF as is , no BP sample

Configuration	% Change in tan(δ)	% Change in Storage Modulus
CF as is, ZnO on BP	60.61	555.82
ZnO on CF, no BP	-14.23	273.98
ZnO on CF, BP as is	90	366
CF and BP as is	41.98	395.93

Frequency Scan Graphs

The DMA test provides the viscoelastic properties of materials when subjected to cyclic loading, namely the storage modulus (dynamic stiffness E'), loss modulus (energy dissipation E") and the tangent of phase angle (E'/E"). Depicted in Figures 4.14, 4.15, 4.16 are the tan (δ) and of the five different composites configurations, under 30°C, 55°C and 80°C, respectively, within frequency range of 1-100 *Hz*.

Evident by Figure 4.14 , at 30°C, a composite that incorporates Bucky paper and ZnO nanowires attained highest increase in tan (δ); an increase by 77% followed by the composite that contains Bucky paper alone (65% increase) and a composite with ZnO grown over the carbon fiber with Bucky paper in between the layers (17.11% increase). The composite with ZnO only did not attain improvements in tan (δ) which is again attributed to insufficient drying of the fibers upon ZnO growth. This drop can also be attributed to the relative

mobility of the nanowires inside the matrix, which, despite enhancing the interfacial inter-action, reduces the composite ability to dissipate mechanical energy.

The increase in tan (δ) demonstrates the capability of the Bucky paper and ZnO nanowires combination, as fiber / matrix reinforcements, to promote the energy dissipation within the material. The energy dissipation in the composite is influenced by the epoxy matrix more than the fibers due to the inherent viscoelastic nature of the polymeric matrix. Besides the matrix contribution, vibrational energy can be dissipated through slippage and frictional interactions between the nano-reinforcement and the matrix. The small size nanowires and the MWCNTs in the Bucky paper yield large reinforcement-matrix interface, thereby enhancing the energy dissipation due to interfacial friction during vibration. As the temperature increases to 55°C, Figure 4.15, some samples; namely with ZnO grown on Bucky paper did not show improvements in tan (δ) indicating that the epoxy matrix underwent further curing. Having two nanofillers will interfere negatively with the curing process, which explains the slight drop in tan (δ). Samples with Bucky paper in general showed improvements in tan (δ) as the Buck paper adheres better to the epoxy than ZnO. Upon heating the sample at 80°C, the composite retained the same trend of tan (δ)as it was at 30°C indicating that no further curing is possible beyond that temperature which is close to the glass transition of the epoxy.

The trend for the storage modulus at 30°C which is an indicative of the viscoelastic stiffness is shown in Figure 4.17. The composite incorporating ZnO nanowires on Bucky-paper exhibited 200% increase in the storage modules compared to the baseline composite with no nanofillers. All the composites with one or two nanofillers showed improvements

of at least 90%. It is worth noting that unlike tan (δ), the storage modulus shows little variation over the frequency range. The same frequency-dependent pattern was observed for all the different composite configurations. It can be also discerned from Figures 4.18 and 4.19 that even at 55°C and 80°C , the same trend holds as far as the composite with ZnO grown on Bucky paper achieving the largest enhancement in the storage modulus. In general, as the temperature increases- like the stiffness- the storage modulus decreases.
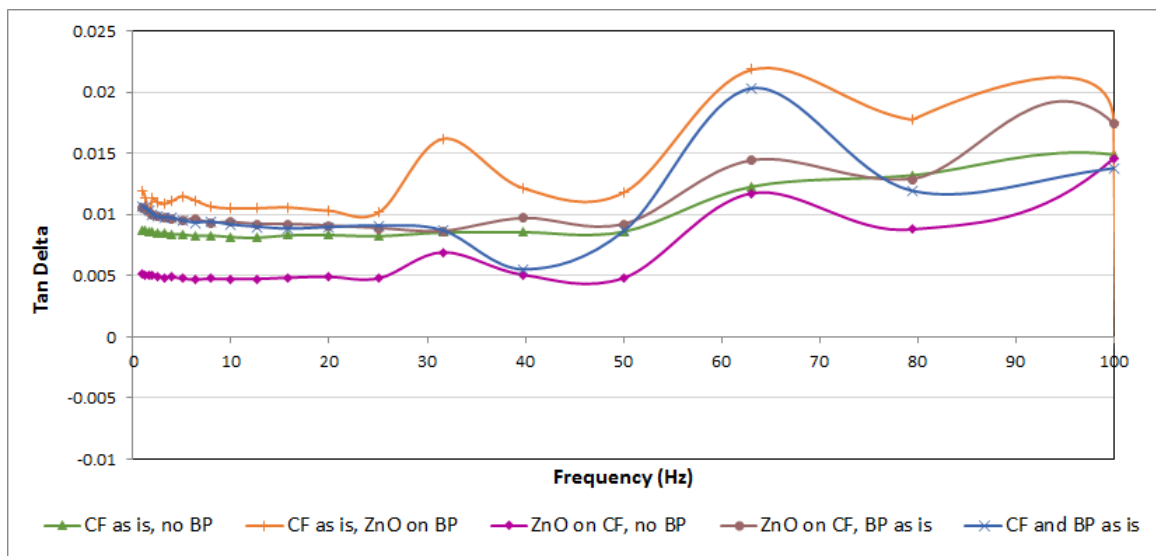
Figure 4.14: Graph showing the variation of tan (δ) with frequency at 30°C for various configurations of two layer composite samples
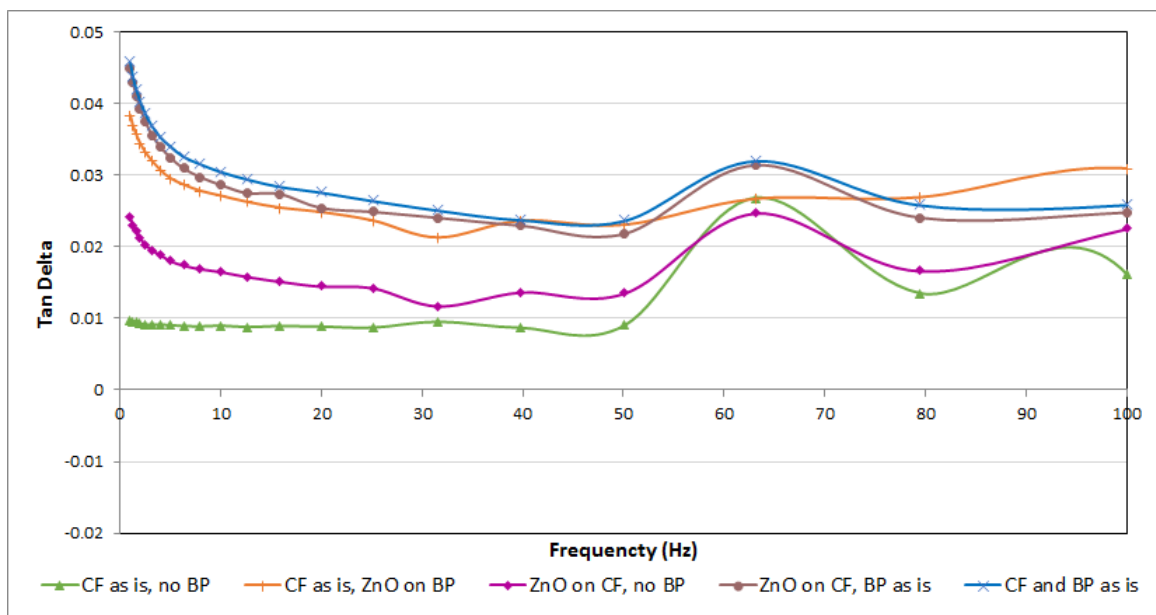
Figure 4.15: Graph showing the variation of tan (δ) with frequency at 55°C for various configurations of two layer composite samples
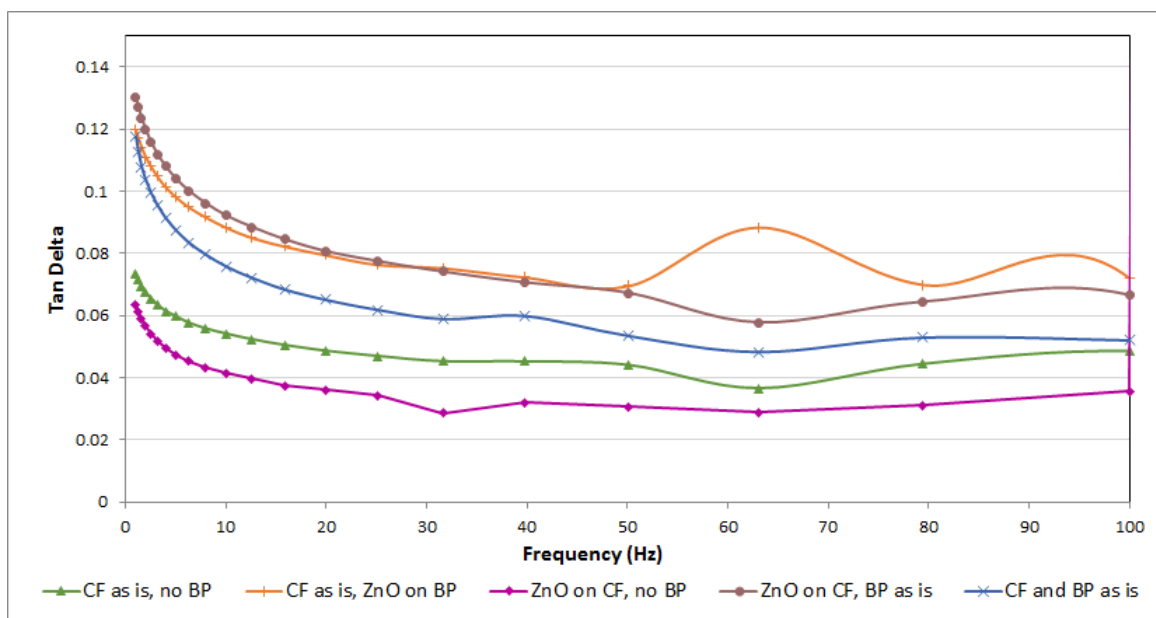
Figure 4.16: Graph showing the variation of tan (δ) with frequency at 80°C for various configurations of two layer composite samples
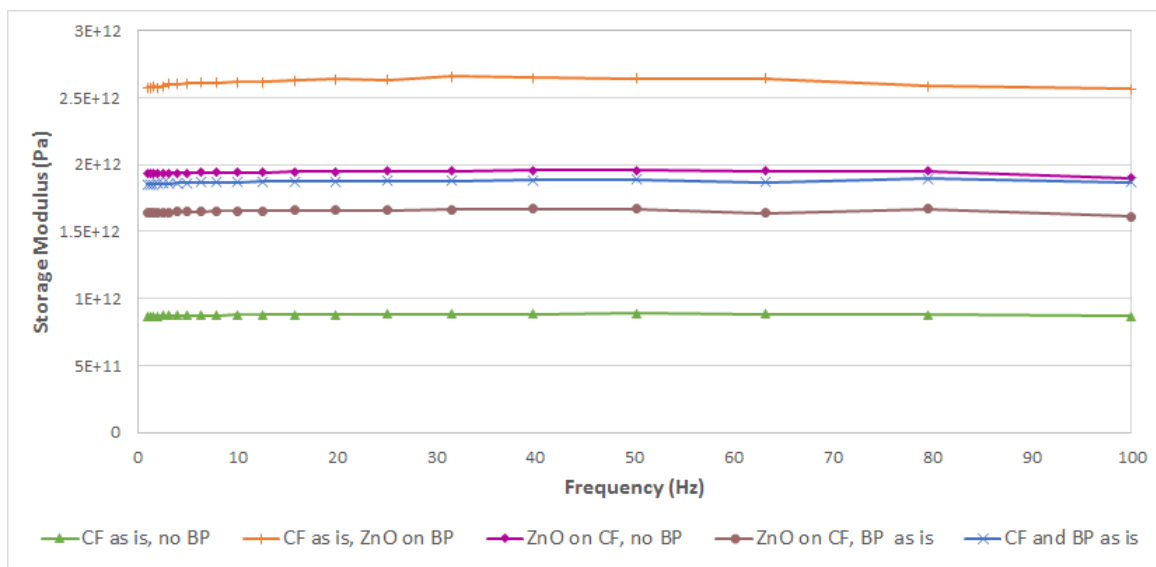
Figure 4.17: Graph showing the variation of storage modulus with frequency at 30°C for various configurations of two layer composite samples
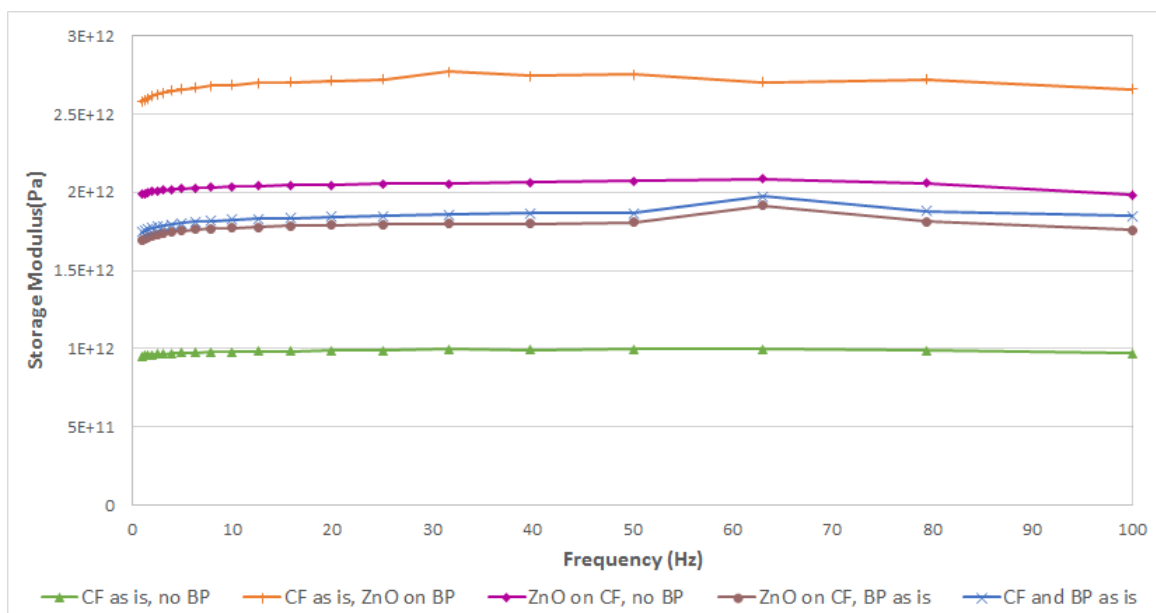
Figure 4.18: Graph showing the variation of storage modulus with frequency at 55°C for various configurations of two layer composite samples
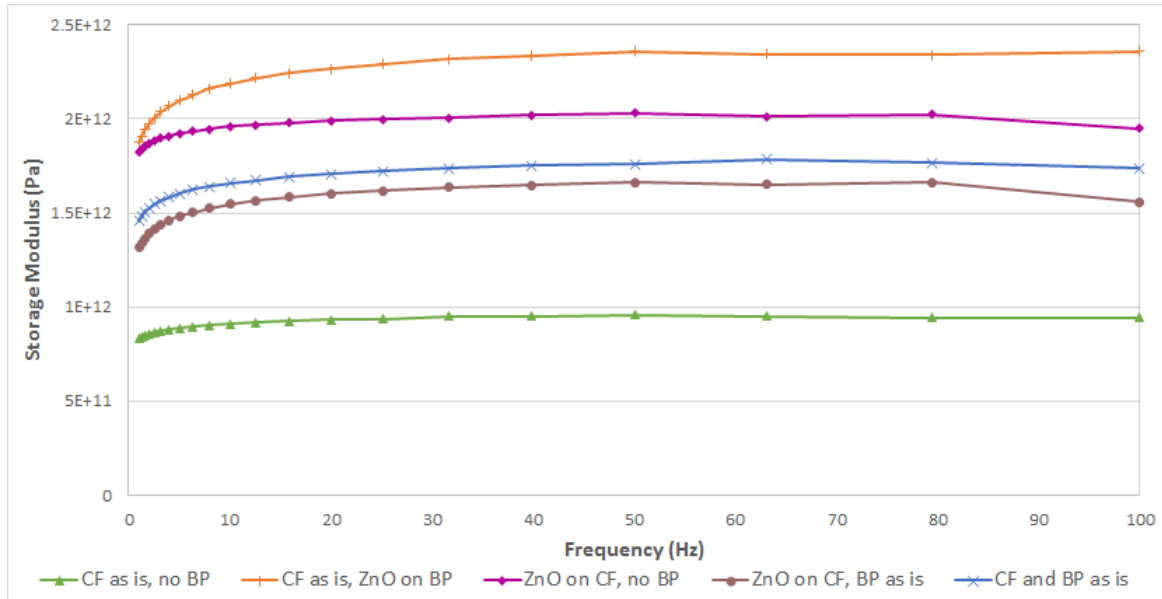
Figure 4.19: Graph showing the variation of storage modulus with frequency at 80°C for various configurations of two layer composite samples

Table 4.3: Comparison with respect to the original CF as is , no BP sample at 30°C

Configuration	% Change in tan(δ)	% Change in Storage Modulus
CF as is, ZnO on BP	77.68	202.86
ZnO on CF, no BP	-4.58	122.86
ZnO on CF, BP as is	17.11	90.86
CF and BP as is	64.85	116

Table 4.4: Comparison with respect to the original CF as is , no BP sample at 55°C

Configuration	% Change in tan(δ)	% Change in Storage Modulus
CF as is, ZnO on BP	-0.48	170.54
ZnO on CF, no BP	-7.76	108.42
ZnO on CF, BP as is	17.16	91.38
CF and BP as is	19.47	97.39

Table 4.5: Comparison with respect to the original CF as is , no BP sample at 80°C

Configuration	% Change in tan(δ)	% Change in Storage Modulus
CF as is, ZnO on BP	141.98	146.29
ZnO on CF, no BP	-20.93	111.23
ZnO on CF, BP as is	57.92	73.50
CF and BP as is	32.08	87.52

4.2.4 Surface Resistivity Comparison

The surface resistivity (SR) of one sample of each configuration was measured. The

data obtained was as follows:

Table 4.6: The trend of surface resistivity for various configurations of two layer
composite samples

Configuration	Length(mm)	Width(mm)	Resistance($ohms$)	SR($ohms/mm^2$)
CF as is, no BP	56.21	5.71	19	187.04
CF as is, ZnO on BP	56.46	6.51	3.93	34.08
ZnO on CF, no BP	66.11	5.17	7.5	95.90
ZnO on CF, BP as is	66.71	6.62	4.67	47.06
CF and BP as is	66.78	5.6	4.12	50.60
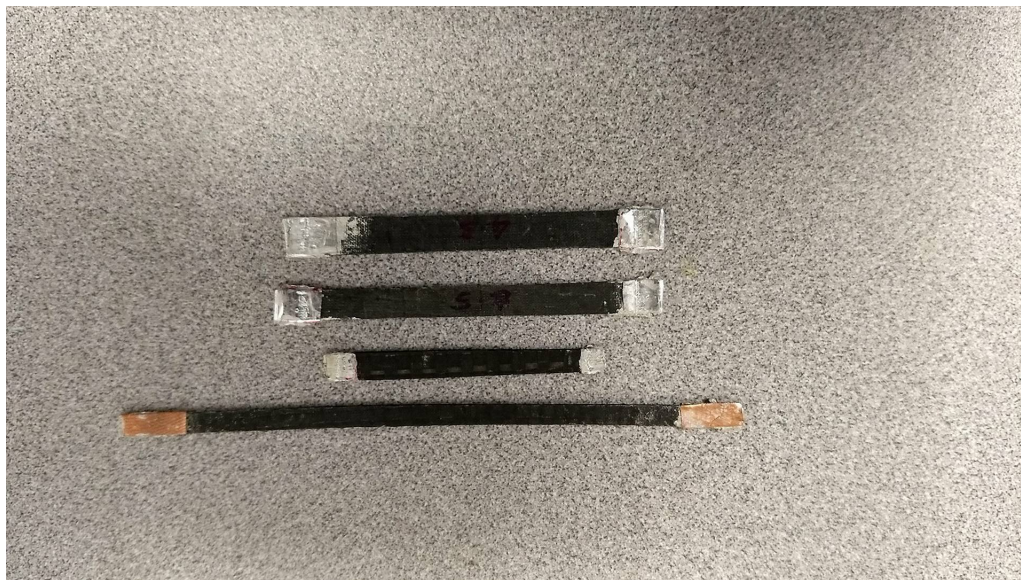
Figure 4.20: Electrical Resistivity Samples

To quantify the improvements of the electrical conductivity, the surface electrical resistivity was measured along the in-plane direction. The results were normalized by the surface area as illustrated in Table 4.6. In comparison to the baseline composite with no nanofillers, the sample with highest measurable conductivity (or least resistivity) was the sample with the ZnO nanowires grown over the surface of Bucky paper. This sample exhibited 82% improvements in conductivity followed by the samples that have ZnO grown over carbon fiber with Bucky paper in between the two laminae (increase by 75%) and the sample with Bucky paper with no ZnO (72%). These results suggest the presence of Bucky paper as a conductive phase plays larger role than that for ZnO, which is a semiconductor. Nevertheless, the sample based on ZnO also exhibited a 49% decrease in resistivity. Hence, one conclude that the presence of a nanophase such as MWCNTs (in Bucky paper) or ZnO

nanowires or both assist in forming continuous conductive pathways which translates to better conductivity.

Table 4.7: Comparison with respect to the original CF as is , no BP sample

Configuration	% Change in Electrical Resistivity
CF as is, ZnO on BP	-81.78
ZnO on CF, no BP	-48.72
ZnO on CF, BP as is	-74.84
CF and BP as is	-72.95

5. Conclusion

This work was an attempt to make new hybrid composite with the best combination of Bucky paper, ZnO nanowires, carbon fiber and epoxy at low temperatures. Several experiments were performed to grow ZnO nanowires on various substrates utilizing a hydrothermal synthesis procedure. The various substrates included silicon, carbon fiber and Bucky paper. Dipping technique in a homogenized solution of zinc acetate, ethanol and deionised (DI) water was used as for seeding purposes. A chemical bath comprising zinc acetate dihydrate, hexamethylenetetramine and DI water in measured concentrations was prepared to provide appropriate catalysts and enzymes to accommodate the growth of nanorods. A very low temperature of $90°C$ was chosen during the synthesis.

Synthesis was followed by composite preparation. Composites of five different configurations were made: CF as is, no BP; CF as is, ZnO on BP; ZnO on CF, no BP; ZnO on CF, BP as is; and CF and BP as is. Characterization using tensile test, fracture analysis, dynamic mechanical analysis was performed for each. Also, surface resistivity was calculated to compare the electrical conductivity among various configurations.

It was observed that delamination results in significant decrease in strength and stiffness of CFRPs. Also, Buckypaper is well known for its poor impregnation with epoxy while employing pressure based techniques for composite fabrication. Thus, CF and BP as is, with no ZnO nanorods showed 14% decrease in stiffness and 1.69% decrease in strength

compared to the original CF as is, no BP composite. In this research, ZnO nanorods were seen to act as z-pinning hurdles, resisting crack propagation and thus helping the composite to withstand higher loads. Thus, CFRPs with ZnO on Bucky paper or on carbon fiber were seen to be more ductile with enhanced strength and stiffness. The largest enhancement in stiffness was 3.36% in ZnO on CF, BP as is hybrid composite, while the highest strength enhancement was seen in CF as is, ZnO on BP hybrid composite by 23.26%.

The results of the fracture analysis validated the z-pinning effect of the ZnO nanorods. The samples with nanofillers showed predominant matrix failure, while the other samples showed both matrix and fiber failure. Temperature scan during the DMA analysis showed a reduction in glass transition temperature of few samples indicating that the filler influenced the epoxy cure reaction kinetics. To further explain this behavior, kinetics studies is to be performed. Increase in tan (δ) was seen in all the samples expect for one configuration where 9% drop was seen. This was attributed to possible insufficient drying of fibers. The storage modulus trend was comparable to the stiffness trend seen during tensile testing with one exception. The sample with carbon fiber and Bucky paper showed higher storage modulus in comparison to raw composite as DMA loading was not high enough to cause premature delamination.

Frequency scan was also performed at 30°C, 55°C and 80°C with frequency values ranging from 1-100Hz. Tan (δ) trends at 30°C and 55°C were similar, while the different trend at 55°C was attributed to curing of epoxy. Enhancement in tan (δ) was because of the promotion of energy dissipation, resulting from the large reinforcement matrix interface formed by the presence of both MWCNTs in Bucky paper and ZnO nanowires. Stor-

age modulus shows insignificant variation over the frequency range unlike tan(δ). Also, nanofillers on Bucky paper showed a 200% increase compared to the raw composite. Other nanofiller configurations also showed a singnificant increase in storage modulus. With increase in temperature, storage modulus was seen to decrease. Finally, conductivity was increased by 82% on the sample with ZnO nanowires on Bucky paper sandwiched between two carbon fiber laminae. Also, the sample with just ZnO nanowires showed a 49% increase in conductivity. This proves that both nanofillers and MWCNTs in Bucky paper aid in charge dissipation in structures.

Thermal and kinetic analysis can further be performed to observe the heat dissipation trends and explain the effects seen due to curing of epoxy.

REFERENCES

Akgun, M. C., Kalay, Y. E., & Unalan, H. E. (2012). Hydrothermal zinc oxide nanowire growth using zinc acetate dihydrate salt. *Journal of Materials Research*, *27*(11), 1445-1451.

Alberto, M. (2013). *Introduction of fibre-reinforced polymers-polymers and composites:concepts, properties and processes.*

Al-Haik, M., Luhrs, C. C., Reda Taha, M. M., Roy, A. K., Dai, L., Phillips, J., & Doorn, S. (2010). Hybrid carbon fibers/carbon nanotubes structures for next generation polymeric composites. *Journal of Nanotechnology*, *2010*, 9.

Allaoui, A., Bai, S., Cheng, H. M., & Bai, J. B. (2002). Mechanical and electrical properties of a mwnt/epoxy composite. *Composites Science and Technology*, *62*(15), 1993-1998.

Ashrafi, B., Guan, J., Mirjalili, V., Hubert, P., Simard, B., & Johnston, A. (2010). Correlation between young's modulus and impregnation quality of epoxy-impregnated swcnt buckypaper. *Composites Part A : Applied Science and Manufacturing*, *41*(9), 1184-1191.

Boskovic, B. O., Golovko, V. B., Cantoro, M., Kleinsorge, B., Chuang, A. T. H., Ducati, C., . . . Johnson, B. F. G. (2005). Low temperature synthesis of carbon nanofibres on carbon fibre matrices. *Carbon*, *43*(13), 2643-2648.

Byrne, D., McGlynn, E., Cullen, J., & Henry, M. O. (2011). A catalyst-free and facile route to periodically ordered and c-axis aligned zno nanorod arrays on diverse substrates. *Nanoscale*, *3*(4), 1675-82. (Byrne, Daragh McGlynn, Enda Cullen, Joseph Henry, Martin O eng Research Support, Non-U.S. Gov't England 2011/02/18 06:00 Nanoscale. 2011 Apr;3(4):1675-82. doi: 10.1039/c0nr00919a. Epub 2011 Feb 15.)

Deka, B. K., Hazarika, A., Kong, K., Kim, D., Park, Y.-B., & Park, H. W. (2016). Interfacial resistive heating and mechanical properties of graphene oxide assisted cuo nanoparticles in woven carbon fiber/polyester composite. *Composites Part A: Applied Science and Manufacturing*, *80*, 159-170.

Demes, T., Ternon, C., Riassetto, D., Stambouli, V., & Langlet, M. (2016). Comprehensive study of hydrothermally grown zno nanowires. *Journal of Materials Science*, *51*(23), 10652-10661.

Dong, J. J., Zhen, C. Y., Hao, H. Y., Xing, J., Zhang, Z. L., Zheng, Z. Y., & Zhang, X. W. (2013). Controllable synthesis of zno nanostructures on the si substrate by a hydrothermal route. *Nanoscale Research Letters*, *8*. (ISI Document Delivery No.: 226FV Times Cited: 9 Cited Reference Count: 30 Dong, Jing-Jing Zhen, Chun-Yang Hao, Hui-Ying Xing, Jie Zhang, Zi-Li Zheng, Zhi-Yuan Zhang, Xing-Wang Fundamental Research Funds for the Central Universities [2652013067] This work was financially supported by 'the Fundamental Research Funds for the Central Universities' (grant no. 2652013067). Springer New york)

Ehlert, G. J., & Sodano, H. A. (2009). Zinc oxide nanowire interphase for enhanced interfacial strength in lightweight polymer fiber composites. *ACS Applied Materials Interfaces*, *1*(8), 1827-1833.

Erik, T. T., & Tsu-Wei, C. (2002). Aligned multi-walled carbon nanotube-reinforced composites: processing and mechanical characterization. *Journal of Physics D: Applied Physics*, *35*(16), L77.

Fu, Y. Q., Luo, J. K., Du, X. Y., Flewitt, A. J., Li, Y., Markx, G. H., . . . Milne, W. I. (2010). Recent developments on zno films for acoustic wave based bio-sensing and microfluidic applications: a review. *Sensors and Actuators B: Chemical*, *143*(2), 606-619.

Garcia, E., Wardle, B., deVilloria, R., Guzman de Villoria, R., Wicks, S., Ishiguro, K., . . . Hart, A. (2008). Aligned carbon nanotube reinforcement of advanced composite ply interfaces. In *49th aiaa/asme/asce/ahs/asc structures, structural dynamics, and materials conference, 16th aiaa/asme/ahs adaptive structures conference,10th aiaa non-deterministic approaches conference, 9th aiaa gossamer spacecraft forum, 4th aiaa multidisciplinary design optimization specialists conference.* American Institute of Aeronautics and Astronautics. (doi:10.2514/6.2008-1768)

Garmestani, H., Al-Haik, M. S., Dahmen, K., Tannenbaum, R., Li, D., Sablin, S. S., & Hussaini, M. Y. (2003). Polymer-mediated alignment of carbon nanotubes under high magnetic fields. *Advanced Materials*, *15*(22), 1918-1921.

Gbaguidi, A., Namilae, S., & Kim, D. (2017). Monte carlo model for piezoresistivity of hybrid nanocomposites. *Journal of Engineering Materials and Technology*, *140*(1), 011007-011007-11. (10.1115/1.4037024)

Gibson, R. F. (2010). A review of recent research on mechanics of multifunctional composite materials and structures. *Composite Structures*, *92*(12), 2793-2810.

Gullapalli, H., Vemuru, V. S. M., Kumar, A., Botello-Mendez, A., Vajtai, R., Terrones, M., . . . Ajayan, P. M. (2010). Flexible piezoelectric zno-paper nanocomposite strain sensor. *Small*, *6*(15), 1641-1646.

Hung, C. H., & Whang, W. T. (2003). A novel low-temperature growth and characterization of single crystal zno nanorods. *Materials Chemistry and Physics*, *82*(3), 705-710. (ISI Document Delivery No.: 753PG Times Cited: 98 Cited Reference Count: 29 Hung, CH Whang, WT Elsevier science sa Lausanne)

Iijima, S. (1991, November). Helical microtubules of graphitic carbon. , *354*, 56-58. doi: 10.1038/354056a0

Jones, R. (1998). *Mechanics of composite materials*. Taylor Francis.

Li, L., Yang, H., Yu, J., Chen, Y., Ma, J., Zhang, J., . . . Gao, F. (2009). Controllable growth of zno nanowires with different aspect ratios and microstructures and their photoluminescence and photosensitive properties. *Journal of Crystal Growth*, *311*(17), 4199-4206.

Li, Y. L., Kinloch, I. A., & Windle, A. H. (2004). Direct spinning of carbon nanotube fibers from chemical vapor deposition synthesis. *Science*, *304*(5668), 276-278. Retrieved from http://science.sciencemag.org/content/sci/304/5668/276.full.pdf

Liu, J., Chang, M.-J., & Du, H.-L. (2016). Controllable growth of highly organized zno nanowires using templates of electrospun nanofibers. *Journal of Materials Science: Materials in Electronics*, *27*(7), 7124-7131.

Lopes, P. E., van Hattum, F., Pereira, C. M. C., Nvoa, P. J. R. O., Forero, S., Hepp, F., & Pambaguian, L. (2010). High cnt content composites with cnt buckypaper and epoxy resin matrix: Impregnation behaviour composite production and characterization. *Composite Structures*, *92*(6), 1291-1298.

Luhrs, C. C., Garcia, D., Tehrani, M., Al-Haik, M., Taha, M. R., & Phillips, J. (2009). Generation of carbon nanofilaments on carbon fibers at 550°c. *Carbon*, *47*(13), 3071-3078.

Ma, Q., Wang, Y., Kong, J., Jia, H., & Wang, Z. (2015). Controllable synthesis of hierarchical flower-like zno nanostructures assembled by nanosheets and its optical properties. *Superlattices and Microstructures*, *84*, 1-12.

Otsuka, K., Abe, Y., Kanai, N., Kobayashi, Y., Takenaka, S., & Tanabe, E. (2004). Synthesis of carbon nanotubes on ni/carbon-fiber catalysts under mild conditions. *Carbon*, *42*(4), 727-736.

Pal, U., & Santiago, P. (2005). Controlling the morphology of zno nanostructures in a low-temperature hydrothermal process. *The Journal of Physical Chemistry B*, *109*(32), 15317-15321.

Puglia, D., Valentini, L., Armentano, I., & Kenny, J. M. (2003). Effects of single-walled carbon nanotube incorporation on the cure reaction of epoxy resin and its detection by raman spectroscopy. *Diamond and Related Materials*, *12*(3), 827-832.

Scanning electron microscope training module. (n.d.).

Sinnott, S. B., & Andrews, R. (2001). Carbon nanotubes: Synthesis, properties, and applications. *Critical Reviews in Solid State and Materials Sciences*, *26*(3), 145-249.

Standard test method for tensile properties of polymer matrix composite materials. (1995). ASTM D3039/D 3039M.

Strano, V., Urso, R. G., Scuderi, M., Iwu, K. O., Simone, F., Ciliberto, E., … Mirabella, S. (2014). Double role of hmta in zno nanorods grown by chemical bath deposition. *The Journal of Physical Chemistry C*, *118*(48), 28189-28195.

Tak, Y., & Yong, K. J. (2005). Controlled growth of well-aligned zno nanorod array using a novel solution method. *Journal of Physical Chemistry B*, *109*(41), 19263-19269. (ISI Document Delivery No.: 974SQ Times Cited: 330 Cited Reference Count: 40 Tak, Y Yong, KJ Amer chemical soc Washington)

Tao, K., Yang, S., Grunlan, J. C., Kim, Y.-S., Dang, B., Deng, Y., … Wei, X. (2006). Effects of carbon nanotube fillers on the curing processes of epoxy resin-based composites. *Journal of Applied Polymer Science*, *102*(6), 5248-5254.

Tehrani, M., Safdari, M., Boroujeni, A. Y., Razavi, Z., Case, S. W., Dahmen, K., … Al-Haik, M. S. (2013). Hybrid carbon fiber/carbon nanotube composites for structural damping applications. *Nanotechnology*, *24*(15), 155704.

Wagner, R. S., & Ellis, W. C. (1964). Vapor-liquid-solid mechanism of single crystal growth. *Applied Physics Letters*, *4*(5), 89-90.

Wang, Z. L. (2004). *Nanostructures of zinc oxide.*